Thin–Walled Structures 198 (2024) 111763

Contents lists available at ScienceDirect

Thin-Walled Structures

journal homepage: www.elsevier.com/locate/tws

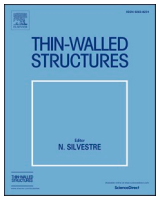

Full length article

Data-driven PSO-CatBoost machine learning model to predict the compressive strength of CFRP- confined circular concrete specimens

Nima Khodadadi [a,*], Hossein Roghani [a], Francisco De Caso [a], El-Sayed M. El-kenawy [b], Yelena Yesha [c], Antonio Nanni [a]

[a] Department of Civil and Architectural Engineering, University of Miami, Coral Gables, FL, 33146, USA
[b] Faculty of Artificial Intelligence, Delta University for Science and Technology, Mansoura, 35712, Egypt
[c] Department of Computer Science, University of Miami, Coral Gables, FL, USA

ARTICLE INFO

Keywords:
PSO-CatBoost
Carbon Fiber-Reinforced Polymer
Confined-concrete
Machine learning
Compressive strength

ABSTRACT

This work articulates the development of a sophisticated machine-learning model for the prediction of compressive strength in Carbon Fiber-Reinforced Polymer Confined-Concrete (CFRP-CC) specimens. Despite extensive empirical studies conducted over the last three decades, prevailing predictive models predominantly rooted in linear or nonlinear regression analyses are constrained by their dependency on limited data scopes. Addressing this deficiency, our research delineates the formulation of an innovative Particle Swarm Optimization- Categorical Boosting (PSO-CatBoost) algorithm, underpinned by an expansive database encompassing 916 experimental outcomes from 105 scholarly articles, spanning the period from 1991 to mid-2023. This innovative approach effectively combines the strengths of Particle Swarm Optimization and the CatBoost algorithm. It carefully evaluates various vital factors that affect the compressive strength of CFRP-CC. The uniqueness of our approach is further accentuated through the application of SHapley Additive exPlanations (SHAP) and Permutation Feature Importance (PFI) methodologies, thereby elucidating the relative importance of each contributory feature. In an unprecedented comparative analysis, the PSO-CatBoost model is rigorously benchmarked against six contemporary machine learning paradigms: CatBoost, XgBoost, AdaBoost, GBoost, Extra Trees, and Random Forest. Furthermore, this model is assessed against six empirical models for further comparison. The model exhibits superior predictive efficacy, evidenced by an exemplary coefficient of determination R-squared of 0.9847, surpassing the methodologies. This research introduces a new predictive model for CFRP-CC and represents a significant shift in concrete research, moving towards a more sophisticated, data-driven, and machine learning-focused methodology. This work thus establishes a new benchmark in the predictive modeling realm for CFRP-CC compressive strength, offering a robust and comprehensive analytical tool for both researchers and practitioners in the field. Lastly, a graphical user interface was designed for modeling the compressive strength of CFRP-CC to facilitate practical use.

1. Introduction

With the rising interest in using FRP in the construction sector, it has become an attractive material to confine concrete columns. In the past three decades, a significant amount of experimental and analytical research has been carried out to comprehend the performance of FRP-CC under compression. There is a general agreement that lateral confinement of concrete columns, which can be FRP wraps for repair and retrofit applications or FRP tubes in new construction, increases ductility and strength by putting the element in the condition of triaxial compression. This hybrid use of FRP and concrete also enhances the durability and service life of these elements [1–7]. The conventional concrete-filled steel tube (CFST) columns are susceptible to steel tube corrosion [8] and delamination failure (steel tube possesses a higher Poisson's ratio than concrete subjected to compression) [9]. The hybrid construction method, utilizing both FRP and concrete, effectively integrates the desirable characteristics of both materials. Concrete contributes mass, stiffness, damping, and cost-effectiveness, while FRP offers advantages such as rapid construction, lightweight, high strength, and long-lasting durability (non-corrosive nature of FRP). FRP is

* Corresponding author.
E-mail address: Nima.khodadadi@miami.edu (N. Khodadadi).

https://doi.org/10.1016/j.tws.2024.111763
Received 27 September 2023; Received in revised form 24 February 2024; Accepted 29 February 2024
Available online 1 March 2024

particularly well-suited for encasing concrete columns due to their orthotropic nature [10,11].

In the case of cylindrical concrete elements subjected to triaxial compressive stresses, primary compressive stresses are applied equally throughout the longitudinal axis of the specimen and lateral confining pressure. When subjected to compression, confined concrete tends to expand in the radial direction. The expansion of the uniaxially loaded FRP jacket generates a reactively confining radial pressure at the interface between the FRP and the concrete. Fig. 1 illustrates the stress patterns resulting from the confining action of FRP on a circular concrete element.

Eq. (1) defines a circular concrete specimen with a diameter of D and confined in FRP wrap or tube with a nominal thickness of t_f, σ_l is confining pressure, σ_f is hoop tensile stress of FRP, and σ_c is the compressive stress [12].

$$\sigma_l = \frac{2t_f\sigma_f}{D} \tag{1}$$

Numerous researchers have investigated using FRP as a confining material for concrete compression members since the 1990s. These studies are divided into two major categories: 1) experimental investigations to provide evidence on the successful use of this confinement technique; and 2) analytical investigations to propose models for predicting the compressive strength and strain of FRP-CC columns for design purposes.

Fig. 2 shows that the initial portion of the stress-strain curve suggests that the FRP confinement has not yet been activated. The term "confining" refers to the activation of FRP confinement through the gradual expansion of the confined concrete. A noticeable turning point could distinguish the two distinct segments. The stress-strain curve of FRP-confined concrete at the confining section may exhibit two primary trends: hardening and softening. The differentiation between the two trends lies in the level of confinement of FRP. The level of confinement of CFRP has a substantial impact on the uniaxial compressive strength of concrete cylinders. The confinement level of CFRP has the potential to significantly enhance the strength of the element [13].

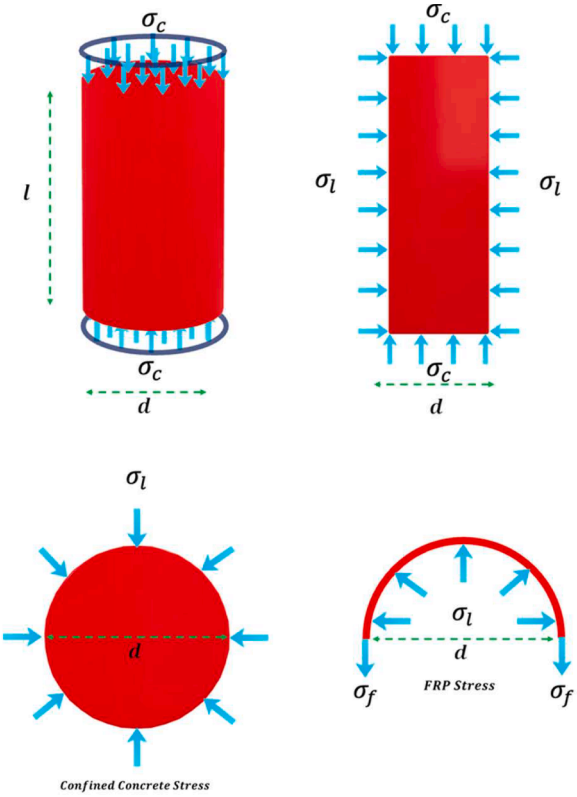

Fig. 1. Schematic view of FRP-confined circular concrete specimen.

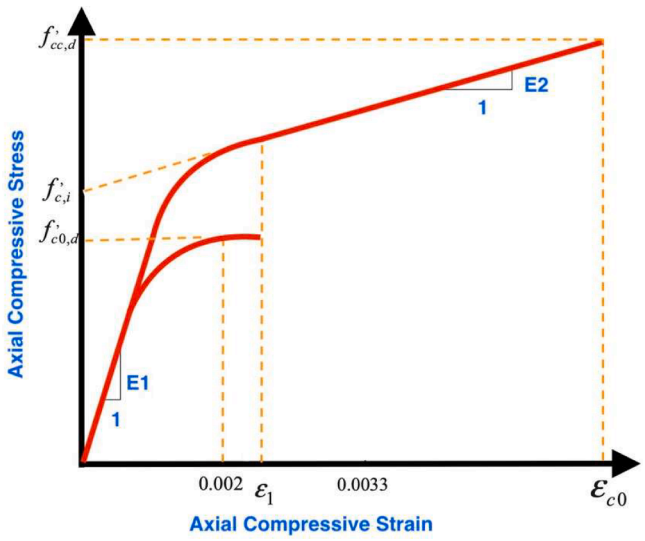

Fig. 2. Stress-strain model of CFRP-confined concrete cylinders.

The behavior of FRP-CC under compression has been well studied through experiments. Mirmiran and Shahawy [10] investigated the behavior of concrete columns with FRP tubes to provide a model for predicting column behavior. The experimental results in this study were compared to the available models, and it was concluded that the models generally overestimate the capacity of columns and lead to dangerous designs. Pessiski et al. [14] studied the performance of FRP-CC columns subjected to a monotonic concentric compressive load. Deformation and load-bearing capacity were observed to be enhanced using an FRP jacket as a confining material.

Several studies were conducted to develop analytical models for predicting the compressive strength of FRP-CC columns. In very early attempts, Samaan et al. [6] provided a model to determine the stress-strain relationship for FRP-encased concrete columns, which is based on the correlation between the hoop stiffness of FRP and the dilatation of concrete. The predicted stress-strain curve by the model agrees with the experiments. In another study, Lam and Teng [5] proposed a model to predict the stress-strain response of FRP-CC, and some critical concerns like the hoop strain of FRP material at rupture, sufficiency of confinement, and effect of FRP stiffness on ultimate strain were resolved in this study. Jian and Teng [15] provided a new model to determine the stress-strain behavior of FRP-CC using a total of 48 data points. In this study, the authors described how the critical factors in a model can impact its precision. It was concluded that their model provides precise predictions, especially for concrete specimens that are weakly confined. Toutanji [16] investigated the behavior of concrete columns with externally bonded FRP wraps. It was observed that FRP confinement could considerably improve ductility, load-bearing capacity, and energy dissipation. The authors proposed a model that provides a reasonable prediction of the stress-strain behavior of the columns. Shahawy et al. [17] evaluated CFRP-wrapped concrete cylinders to validate a proposed confinement model for concrete columns encased with Glass FRP (GFRP) tubes. It was concluded that the model could be used for both types of FRP, glass and carbon, and both applications: FRP wrap for strengthening and FRP tube for new construction.

In recent times, machine learning (ML) methods have gained significant recognition owing to advancements in computer software and the strength of algorithms. A primary benefit of a data-driven ML model is that it doesn't require the user to understand a problem comprehensively. With sufficient data and domain knowledge, an ML model can assist users in predicting outcomes in a complex system [18]. Fig. 3

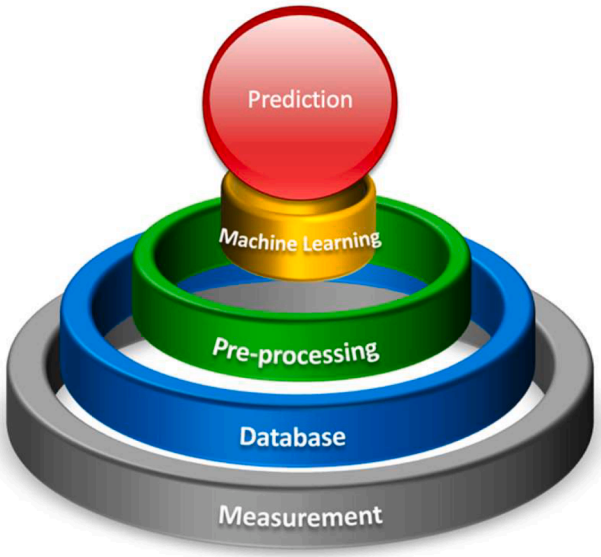

Fig. 3. Prediction process with ML.

illustrates the complete process of creating a machine learning model, from the initial measurement stage (conducting experiments) to the final stage of making predictions.

Zhang et al. [19] investigated the use of Ensemble Learning (EL) algorithms to predict the capacity of FRP-strengthened reinforced concrete beams. This study included four distinct ensemble learning (EL) techniques, specifically random forest, adaptive boosting, gradient boosting decision tree, and extreme gradient boosting. In order to highlight their superiority, these models were compared against representative empirical models as well as those based on single ML methods. The EL-based models exhibited superior performance compared to both the empirical models and the single ML-based models. Hence, the EL-based models suggested in this study exhibit promise for utilization in engineering applications.

Chen et al. [20] conducted a study to examine the application of probabilistic ML approaches in predicting the performance of structures and infrastructure. This study investigated the capabilities of a novel method called natural gradient boosting (NGBoost) for generating probabilistic predictions directly. This output is well-suited for reliability and performance analysis frameworks. It also allows for the use of self-learning algorithms and the optimum design of experiments and field measurement programs in engineering applications. Two specific problems in the field of structural engineering were examined to assess the practicality of NGBoost: (1) predicting the strengths of squat shear walls, and (2) classifying the seismic damage severity for conventional bridges. The findings demonstrate that NGBoost achieves similar levels of mean prediction accuracy as traditional ML algorithms while also offering reliable estimations of prediction uncertainties.

Recently, an interest in using ML-based algorithms to predict the compressive behavior of FRP-CC has been observed. For instance, Berradia et al. [21] developed two prediction models, one using a common form of regression and the other using an Artificial Neural Network (ANN). The database employed in this study included a total of 364 experiments conducted on concrete compressive members. Some statistical indices were employed to carry out statistical analyses and compare the two approaches. The statistical investigation revealed that the ANN model is more efficient and accurate in predicting the strength and strain of FRP-CC specimens strengthened with CFRP wrap. Eight different models were proposed by Kaveh and Khavaninzadeh [22] using a combination of four metaheuristic algorithms and two different ANN approaches to predict the strength of FRP-CC columns. In this study, 233 experimental results were obtained from the literature, with one portion used for the training set and the other for the test data set. Several statistical indices, such as mean squared error, root mean squared error, and the coefficient of determination, were utilized for comparison purposes. The highest accuracy was obtained using a metaheuristic algorithm called enhanced colliding bodies optimization (ECBO) and a neural network called Feed-Forward Backpropagation (FFB). Li et al. [23] proposed a data-driven model based on an ML approach to predict the load-carrying capacity of concrete columns confined with GFRP. A dataset including 114 experimental results was used to develop the model. The back propagation neural network algorithm used in this study provides reasonable fits for training and test data sets and a coefficient of variation of 14.22 %. A sensitivity analysis revealed that the concrete strength and thickness of the FRP composite are the most important parameters affecting the strength of the confined section. Ilyas et al. [24] developed an ML-based model using the multi-expression programming (MEP) algorithm to predict the compressive strength of CFRP-CC. A total of 828 experimental data points were employed to develop the model in this study. The proposed model was compared with existing models in the literature and showed that the ML-based model provided more accurate results.

Keshtegar et al. [25] proposed a hybrid regression and ML model to predict the ultimate strength and strain of FRP-CC systems. The combination of the response surface model (RSM) with support vector regression (SVR) results in the creation of a new hybrid model called RSM-SVR. The predictions generated by the proposed model were compared to those made by six empirical models and two data-driven models of RSM and SVR. The database used for comparison consisted of 780 test results related to circular columns. The statistical analysis demonstrates that the new RSM-SVR model provides more precise predictions for the compressive strength and related axial strain of FRP-CC compared to existing models. The results indicate that both the RSM-SVR and SVR models consistently anticipate the strength and strain enhancement ratios for lateral confining ratios greater than 1, whereas the other models demonstrate chaotic model errors. The proposed model achieves excellent accuracy and reliable predictions by leveraging its exceptional flexibility and soundness in capturing the impact of lateral confining pressure due to the interaction between the concrete core and FRP jacket, compared to the previous models.

The study conducted by Chen et al. [26] examined the utilization of data-driven Bayesian probabilistic and ML prediction models, including back-propagation ANN, multi-gene genetic programming, and support vector machine. Initially, a thorough compilation of 471 test results on the ultimate conditions of FRP-CC cylinders was conducted. Subsequently, a Bayesian parameter estimation technique was employed to construct an updating procedure. This procedure aimed to assess the essential parameters in the current models and subsequently enhance the selected existing models. The database was utilized for generating ML models as well. The proposed models have been verified to demonstrate computational efficiency, transferability, and precision. The results indicate that the suggested Bayesian posterior models, back-propagation artificial neural network, multi-gene genetic programming, and support vector machine models shown exceptional predictive capability, with the support vector machine achieving the best level of accuracy in predictions.

Developing a resilient ML model is widely considered a complex and time-consuming endeavor. The process entails the careful selection of an appropriate algorithm and the development of an efficient model structure through the optimization of hyperparameters [27]. Several algorithms, such as tree-based ML algorithms and deep neural networks, possess multiple hyperparameters that substantially impact the accuracy of predicted values by model [28]. Therefore, the precise adjustment of hyperparameters using an optimization technique holds significant importance. Metaheuristic algorithms, frequently derived from natural phenomena, can comprehensively traverse the search domain while efficiently converging upon a highly satisfactory outcome. These methods can, within a computationally feasible time frame, ascertain

solutions that are either optimal or proximate to optimality for complex problems [29]. The Particle Swarm Optimization (PSO) [30] algorithm is widely employed as a metaheuristic approach that has demonstrated considerable efficacy in addressing various optimization problems.

In this study, an attempt has been made to propose a new ML model based on Particle Swarm Optimization and the Categorical Boosting algorithm (PSO-CatBoost) to predict the compressive strength of CFRP-CC under axial compression using 916 experimental tests from the literature.

Many researchers have conducted comprehensive analyses of experimental data associated with circular concrete specimens, which is the core focus of the current study. CFRP is commonly employed as a composite material in civil engineering applications to repair or strengthen reinforced concrete structural elements. Existing equations for calculating the compressive strength of CFRP-confined circular concrete columns have been developed using regression analysis on a small database. Different optimum design equations have been proposed by various researchers as possible substitutes. Nevertheless, these models are based on limited datasets and rely on simplistic linear or nonlinear regressions or algorithms, making them suitable only for datasets with a narrow range. Numerous researchers in the field of concrete confinement have made efforts to compile databases that serve as essential validation tools for assessing the effectiveness of a model. Therefore, developing a more accurate and robust prediction model that can comprehensively capture the intricate behavior of CFRP-confined circular concrete specimens is imperative. Numerous investigative research projects have been conducted on concrete reinforced with FRP jackets, focusing on creating dependable and precise numerical models for predicting its behavior. However, the majority of these investigations primarily sought to establish analytical models, which were often based on a somewhat narrow scope of experimental findings. A significant concern with these models is their inherent bias and their limited application scope, as they are largely dependent on experimental data derived from studies with varying types of specimens. Since these analytical models are formulated from experimental data, their accuracy is directly tied to the data quality used. To avoid bias in these models, it is essential to utilize comprehensive databases that include specimens with diverse characteristics. The current study has compiled a comprehensive dataset encompassing an extensive range of features. This approach contrasts with other numerical and machine learning models, which typically utilize a limited set of features for model development. The gathered dataset enables a more equitable comparison with existing numerical methods that incorporate a similar breadth of features. Consequently, a fairer and more accurate comparison is facilitated, enhancing the validity of the study's findings. This methodology addresses the constraints observed in previous models, which were based on a more restricted feature set, and offers a more expansive perspective for the assessment of various modeling techniques.

Hence, the primary advancements and contributions of this paper can be summarized as follows:

- This study employed a comparatively extensive dataset on CFRP-CC specimens, leading to more reliable predictions due to the overfitting problem.
- Although the CatBoost algorithm has demonstrated exceptional performance in various ML tasks, more research is needed that explicitly assesses its effectiveness in estimating the compressive strength of CFRP-CC under axial compression.
- CatBoost methods are rarely used in ML issues, although PSO is increasingly used. Concerning prediction accuracy and computing costs, this study evaluates the PSO-CatBoost model's performance for the CFRP-CC problem's compressive strength.
- Six other ML techniques, including CatBoost, XgBoost, AdaBoost, GBoost, Extra Trees, and Random Forest, are compared with the proposed method.
- Six empirical models are compared with PSO-CatBoost.
- PSO-CatBoost showed better results and higher accuracy than different methods.

The rest of this paper is organized as follows: Section 2 introduces existing models of compressive strength relevant to the subject. Section 3 showcases the detailed importance of this study and current compilation of experimental data derived from published research focused on the topic. The development of the PSO-CatBoost model is delineated in Section 4. The model outcomes are discussed in Section 5, broken down into five subsections: setting the performance measures, evaluating the model's performance, comparing with ML methods, performing an analysis of feature significance, and providing a Graphical User Interface. Finally, Section 6 provides the conclusion of the current study.

2. Existing compressive strength of FRP-CC models

This section presents a range of design models previously proposed to determine the compressive strength of CFRP-CC. These models have also been employed for comparison purposes in this study. The rationale for selecting these six particular models is that they lack any parameters that were not taken into account in the model proposed in this study. The following section will present a statistical analysis regarding the precision of these design models. It is important to mention that all models presented in this study are expressed in the International System of Units (S.I. units).

2.1. Mandal et al.'s model

The efficacy of FRP as a confining material for concrete compressive members was investigated by Mandal et al. [31]. The unconfined compressive strength of the concrete varies between 26 and 81 MPa. The experimental component of the investigation involved two large-scale concrete-filled FRP tubes and 59 plain and FRP-wrapped concrete cylinders. The cylinders were encased with either a single layer of GFRP sheet, two layers of GFRP sheet, or a single layer of CFRP sheet. The specimens underwent axial compression testing until they reached the point of failure. The results demonstrated that a considerable improvement in strength could be achieved in low- to medium-strength concrete; strain hardening was also observed in the bilinear strain-stress response, but the strength and ductility improvements for high-strength concrete were insignificant. A model was also proposed considering five parameters: compressive strength of unconfined concrete (f'_{co}), nominal thickness of FRP reinforcement (t_f), effective modulus of elasticity of FRP in hoop direction (E), diameter of compression member (D), and hoop tensile strength of FRP composite (f_u). Eq. (2) shows the proposed model for predicting the peak strength of FRP-confined concrete using analysis of test data (normalized).

$$f'_{cc} = 0.0017 f'_{co}\left(\frac{Et_f}{D/2}\frac{f_u}{f'_{co}}\right)^2 + 0.0232 f'_{co}\left(\frac{Et_f}{D/2}\frac{f_u}{f'_{co}}\right) + f'_{co} \tag{2}$$

The model effectively reflected the reduction in the effectiveness of the confinement provided by FRP as the concrete strength increased.

2.2. Karbhari and Gao's model

Karbhari et al. [32] proposed a model to predict the strength and strain in FRP-CC to facilitate the design of these elements. The key parameters used in the model were unconfined concrete compressive strength (f'_{co}), nominal thickness of FRP composite (t_f), diameter of circular concrete (D), and tensile strength of FRP composite (f_f). The predicted strength and strain by the model are in good agreement with the experimental data. Eq. (3) presents the proposed model for forecasting the ultimate strength of FRP-confined concrete.

$$f'_{cc} = f'_{co} + 2.1 f'_{co}\left(\frac{2f_f t_f}{D f'_{co}}\right)^{0.87} \quad (3)$$

The proposed equation for ultimate strength has a strong correlation with the experimental results in their study.

2.3. Lillistone and Jolly's model

To investigate the impact of FRP confinement on the strength and ductility of the concrete column, Lillistone and Jolly [33] tested a total of 121 columns. The confinement that the FRP provided to the core of the concrete enhanced the strength and ductility of the section. Unconfined concrete compressive strength (f'_{co}), nominal thickness of FRP composite (t_f), tensile modulus of elasticity of FRP (E_f), and diameter of circular concrete column (D) were the five parameters used in this study to develop the analytical model.

$$f'_{cc} = 0.83 f'_{co} + 0.05 f'_{co}\left(\frac{2E_f t_f}{D f'_{co}}\right) \quad (4)$$

2.4. Reza et al.'s model

This model [34] introduces a proposed strength model aimed at determining the maximum axial strength of FRP-confined concrete compression members. Initially, an assessment of existing strength models for evaluating the confining effect on FRP-wrapped concrete specimens was conducted, followed by the creation of an extensive database comprising 520 confined concrete specimens, detailing various geometric and material characteristics. Subsequently, the following model was proposed based on regression analysis:

$$f'_{cc} = f'_{co} + 3 f'_{co}\left(\frac{f_l}{f'_{co}}\right)^{0.75} \quad (5)$$

2.5. Realfonzo and Napoli's model

In this study [35], a comprehensive database is introduced, containing data from compression tests conducted on more than 450 concrete cylinders that were externally reinforced with F materials. Initially, the gathered data was used to carry out a statistical assessment of the FRP strain efficiency factor, with a special focus on examining the impact of the fiber type and the strength of the unconfined concrete. Subsequently, new formulas for predicting the compressive strength of FRP-confined concrete were formulated based on best-fit analyses as follows:

$$f_{cc} = f'_{co} + 3.49 f'_{co}\left(\frac{f_l}{f'_{co}}\right)^{0.86} \quad (6)$$

2.6. Vintzileou and Panagiotidou's model

This research [36] investigates the confinement of concrete using FRP materials, conducting a thorough examination of experimental studies and predictive models for the mechanical behavior of FRP-confined concrete. An empirical model that is suitable for both circular and prismatic elements is introduced, utilizing the principles outlined for confining concrete with hoops or spirals. The model is defined as:

$$f'_{cc} = f'_{co} + 2.8 f'_{co}\left(\frac{f_l}{f'_{co}}\right) \quad (7)$$

In Eqs. (5–7), the parameters include the unconfined concrete compressive strength (f'_{co}), ultimate compressive strength of the unconfined concrete (f'_{cc}), ultimate compressive strength of the confined concrete and ultimate confining pressure (f_l).

The analytical model introduced by Mandal et al. [31] omits consideration of the element's height. Similarly, the framework posited by Karbhari and Gao [32], Reza et al. [34], Realfonzo and Napoli [35] and Vintzileou and Panagiotidou [36] lack an assessment of both the element's height and the elastic modulus of the FRP. Furthermore, the model developed by Lillistone and Jolly [33] did not incorporate the element's height and the FRP's tensile strength. In contrast, the model proposed in the present study integrates the effects of these parameters.

3. Construction of database

The experimental database [37] comprises 916 test data points from 105 studies on FRP-CC specimens. Several parameters related to concrete and FRP geometrical and mechanical characteristics were identified in the literature. Among all the features, seven critical parameters of the data points were used to develop the model: diameter of compression member (D), height of compression member (H), compressive strength of unconfined concrete (f'_{co}), FRP reinforcement ratio (ρ_f), tensile modulus of elasticity (E_f), ultimate tensile strength of FRP (f_f), nominal thickness of FRP reinforcement (t_f), number of FRP layers (*Layers*). In this database, the target value is the compressive strength of confined concrete (f'_{cc}). These parameters are summarized in Table 1. It should be noted that the fiber orientation is not considered as a parameter in the database, later in the model and comparisons.

Normalization is an essential preprocessing step in the field of machine learning because it effectively addresses the issue of scale sensitivity that many algorithms encounter. This is particularly relevant for algorithms that rely on distance measures or gradient descent methods. The utilization of symmetry in the loss surface facilitates expedited model training, leading to accelerated convergence of the optimizer. Furthermore, it enhances comprehension of the significance of features and guarantees numerical stability in mathematical calculations. All input and output variables (x_i) in the database are normalized. The formula to normalize data to a range between -1 and 1 is as follows:

$$x_{i,normal} = 2 \times \left[\frac{x_i - min\ (x)}{Max(x) - Min(x)}\right] - 1 \quad (8)$$

where x_i is the original value, *Min* and *Max* is the minimum and maximum value in each feature in the dataset. In this formula, $(x_i - min\ (x))\ /\ (Max(x) - Min(x))$ normalizes x_i into a range of [0,1], and $2 \times (x_i - 0.5)$ maps the range from [0,1] to [-1,1]. By subtracting 0.5 from each normalized value, you center the range around 0, making it [-0.5, 0.5]. Then, multiplying by 2 scales the range to [-1, 1]. This results in the new normalized dataset having values between -1 and 1.

The database only includes studies on circular concrete specimens without any internal or external reinforcement other than the FRP wraps or FRP tubes. The height-to-diameter ratio of specimen is less than or equal 5, the specimens were subjected to a monotonic concentric compressive load, and the failure mode in all specimens was FRP rupture. The following terms are used in the database tables:

■ CFRP: Carbon fiber reinforced polymer

Table 1
Geometric and material properties of FRP-confined specimens.

Group	Notation	Description	Unit
Specimen geometry	D	Diameter of compression member	*mm*
	H	Height of compression member	*mm*
Concrete	f'_{co}	Compressive strength of unconfined concrete	*MPa*
FRP properties	ρ_f	FRP reinforcement ratio	–
	E_f	Tensile modulus of elasticity of FRP	*GPa*
	f_f	Ultimate tensile strength of FRP	*MPa*
	t_f	Nominal thickness of FRP reinforcement	*mm*
	Layers	Number of FRP layers	–
Result	f'_{cc}	Compressive strength of confined concrete	*MPa*

- HM CFRP: High modulus CFRP
- UHM CFRP: Ultra-high modulus CFRP
- C-Type: Concrete Type (L: low, N: Normal, H: High)

Limiting the database with these criteria helps to reduce the inconsistencies in the predicted values by the model; for instance, restricting the height-to-diameter ratio reduces the discrepancies in the type of failure due to the slenderness of the specimen. The concrete used in these experiments covers a wide range of concrete strengths, from 6.2 MPa, low-strength concrete, to 169.7 MPa, high-strength concrete. In these studies, different CFRP composites were used with a modulus of elasticity ranging from 16 GPa to 640 GPa, ultimate tensile strength from 174 MPa to 4900 MPa, a reinforcement ratio from 0.001 to 0.082, and a total nominal thickness of 0.09 mm to 5.84 mm. The compressive strength of confined concrete in all these tests ranged from 12.8 MPa to 303.6 MPa. The minimum/maximum, mean value, and standard deviation for all seven features are represented in Table 2.

There are a total of 800 data points on CFRP-wrapped concrete specimens and 116 on CFRP-filled concrete tubes. There are a total of 23 data points with a compressive strength of unconfined concrete lower than 15 MPa (L), 687 data points with a strength between 15 MPa and 55 MPa (N), and 206 data points with a strength above 55 MPa (H) (classification according to ACI 318–19 [38]). There is a total of 825 data points with the CFRP modulus of elasticity ranging lower than 340 GPa (CFRP), 73 data points with strength between 340 GPa and 520 GPa (HM_CFRP), and 18 data points with strength above 520 GPa (UHM_CFRP) (classification according to ACI 440.2R-17 [39]). This information is summarized in Table 3. Fig. 4 illustrates the distribution of input and output parameters, their frequency of occurrence within the dataset, and the correlation existing between these parameters.

The database is presented in a supplementary file and is accessible through the link provided in Appendix A. at the end of this paper. The database is summarized in Tables 4 and 5 for FRP-wrapped and FRP tube-encased, respectively.

4. Construction of the model

Gradient Boosted Decision Trees (GBDTs), an ensemble method based on decision trees, were first introduced by Friedman [135]. They have garnered considerable attention in rival data science due to their outstanding efficacy in a wide range of ML tasks [136]. GBDTs employ the boosting methodology to construct a robust learner by integrating multiple weak learners, each exhibiting relatively low accuracy on its own. This study is focused on one of the GBDT variations, namely Categorical Boosting (CatBoost), which is improved to generate a prediction model.

4.1. Categorical boosting (CatBoost)

The CatBoost algorithm [137], the ML technique built upon GBDTs, can be utilized for various machine learning tasks, including binary or multi-class classification and regression. CatBoost stands out from other prominent GBDT algorithms due to several noteworthy algorithmic advancements. The developments encompass the implementation of a

Table 2
Statistical range of database parameters.

Parameter	Minimum	Maximum	Mean	Standard deviation
H/D	1.6	5	2	0.36
f'_{co} (*MPa*)	6.2	169.7	45.47	24.8
ρ_f	0.001	0.082	0.015	0.015
E_f (*GPa*)	16	640	222.87	101.99
f_f (*MPa*)	174	4900	3145.8	1212.1
t_f (*mm*)	0.09	5.84	0.58	0.65
Number of Layers	1	12	2.45	1.65
f'_{cc} (*MPa*)	12.8	303.6	86.3	40.8

Table 3
Classification of database.

Confinement type	CFRP type	Concrete classification	No. of data points
Wrap	CFRP	L	22
		N	581
		H	120
	HM CFRP	L	0
		N	40
		H	29
	UHM CFRP	L	0
		N	8
		H	0
Tube	CFRP	L	1
		N	50
		H	51
	HM CFRP	L	0
		N	4
		H	0
	UHM CFRP	L	0
		N	4
		H	6
Total experiments		916	

structured boosting framework and a novel algorithm for handling categorical features [138]. In conventional gradient-boosting decision trees, estimating the gradient and constructing the model depends on utilizing identical samples [139]. As a result, GBDT algorithms exhibit a prediction shift in the resultant model, which gives rise to a specific form of target leakage issue [140]. To tackle this matter, the CatBoost methodology utilizes the innovative ordered boosting framework, which effectively mitigates gradient estimation bias and minimizes algorithmic complexity. The CatBoost algorithm also places significant importance on the support of categorical features. In contrast to traditional boosting algorithms, which necessitate preprocessing procedures such as one-hot encoding or transforming categorical features into gradient statistics, CatBoost employs an intelligent preprocessing technique that involves modified target statistics. This technique uses random permutations to determine the feature value of specific instances, utilizing information from other cases. The process is iterated multiple times, and the results are averaged [141]. The implementation of these steps is successful in mitigating overfitting and substantially improving the efficiency of the CatBoost model. CatBoost is unique among GBDT-based algorithms since it employs "oblivious trees," a variant of decision trees that are both symmetric and balanced and apply the same splitting rule at every level of the tree. During testing, Oblivious Trees dramatically increase execution speed while being less prone to overfitting [142].

4.2. Particle swarm optimization (PSO)

Particle Swarm Optimization (PSO) was created by Eberhart and Kennedy [30]. Random assignment is used during the initialization phase of this technique. The population members are commonly denoted as particles, with each particle initially allocated a velocity. PSO is a computational technique replicating the cooperative foraging behavior observed in various species such as insects, fish, and birds. In these species, swarms work together to search for food resources [143]. The conceptual basis of PSO is characterized by its simplicity, facilitating its coding and implementation processes.

Moreover, PSO exhibits advantageous computational properties, such as low memory usage and minimal CPU time requirements. In PSO, a particle is utilized as a potential solution representing a specific point within the search space. This particle continuously modifies its flight trajectory by considering its fitness and velocity values. The objective is to gradually approach the most favorable experiences of the entire swarm, with final aim of locating the global optimum within the solution space of D dimensions. The PSO algorithm has garnered considerable interest and has demonstrated successful applications across diverse domains, particularly addressing unconstrained continuous

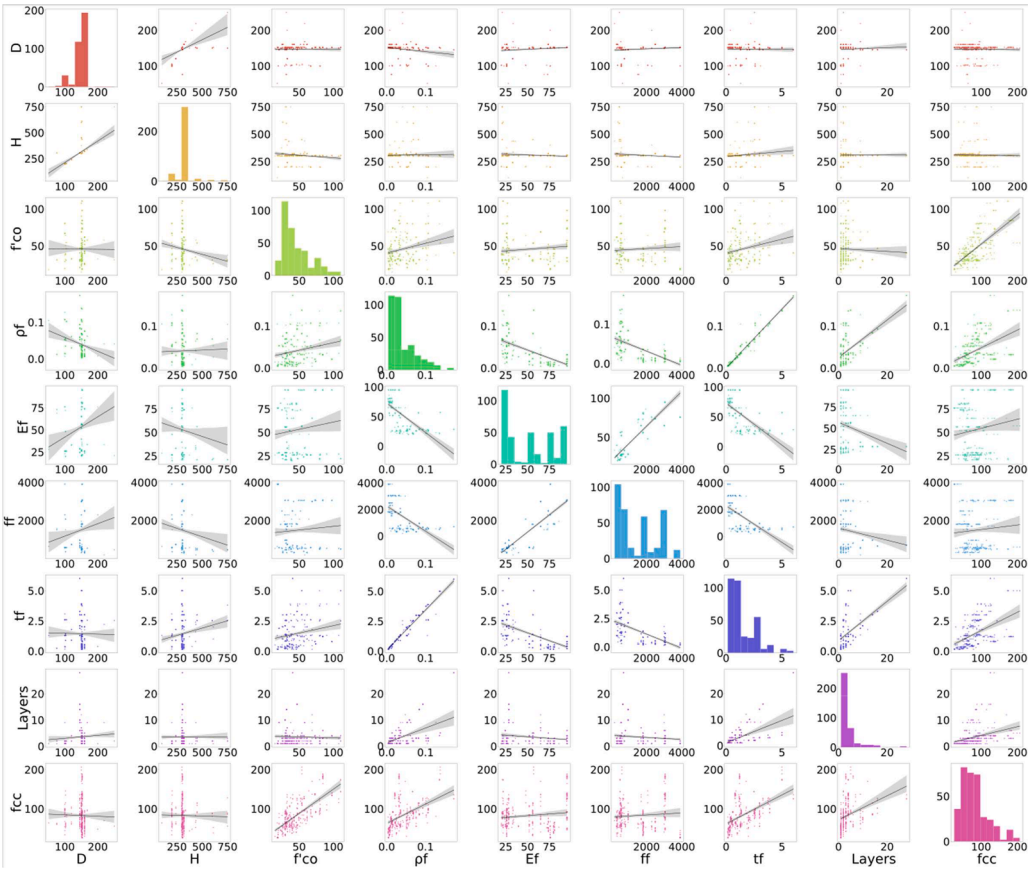

Fig. 4. Multi-correlation among input and output variables.

optimization problems.

In a search space with multiple dimensions, denoted as d, the position and velocity of each particle at a given time t are represented as $X_i^t = (x_{i,1}^t, x_{i,2}^t, x_{i,3}^t, ..., x_{i,d}^t)$ and $V_i^t = (v_{i,1}^t, v_{i,2}^t, v_{i,3}^t, ..., v_{i,d}^t)$ respectively. During each stage of evolution, X_i^t and V_i^t are adjusted by taking into account the impact of personal best experience (P_{best}) and global best experiences (G_{best}), as illustrated in the following equation.

$$X_i^{t+1} = X_i^t + V_i^{t+1} \tag{8.1}$$

$$V_i^{t+1} = w^t.V_i^t + c_1.r_1.\left(P_{best\ i}^{\ t} - X_i^t\right) + c_2.r_2.\left(G_{best}^{\ t}\right) \tag{8.2}$$

In this context, the consideration involves the inclusion of acceleration constants c_1 and c_2, random variables r_1 and r_2 that have values within the range of 0 and 1, and the inertia weight w^t, which governs the alterations in velocity.

4.3. Particle swarm optimization- categorical boosting (PSO-CatBoost)

The optimization of hyperparameters plays a crucial role in the field of ML as it directly impacts the functioning of training algorithms [144]. Basic strategies such as Random Search (RS) and Grid Search (GS) can be utilized to carry out hyperparameter tuning; however, each of these approaches has a number of drawbacks that must be taken into consideration [145]. Some of these drawbacks include the presence of complex search spaces, the requirement for more time for each iteration, and the presence of high variance. Furthermore, the PSO technique, a metaheuristic optimization approach based on swarm intelligence, offers the advantage of being straightforward to implement while efficiently identifying optimal solutions within a multidimensional search space that closely corresponds to the actual solutions. This study employed the PSO algorithm to determine the optimal hyperparameters for the CatBoost algorithms. The Pseudo code of PSO-CatBoost is depicted in Fig. 5. The basic PSO algorithm is influenced by several control parameters, including fitness criteria such as Mean Square Error (MSE) as well as the local coefficient (c_1), global coefficient (c_2), inertia coefficient (w), maximum iteration count (max_{iter}), and population/swarm size (s). This study determined the initial parameter setting in the PSO algorithm through a series of trial-and-error tests.

The initial step in constructing the PSO-CatBoost model involved identifying optimal hyperparameters by utilizing the PSO algorithm. Hence, the optimization algorithm was employed to ascertain the crucial and efficacious hyperparameters, precise depth, learning rate, and L2-regularization. Following the PSO process, the optimal values for the parameters depth, learning rate, and L2-regularization were determined.

The architectural detail of the PSO-CatBoost model is shown in Fig. 6. As shown in this figure, pre-processing the data, defining the features and target, training data by splitting it into two sets of data, optimizing the hyperparameters for CatBoost by PSO, and evaluating the data model are the main modules for this model.

5. Results and discussion

This section utilizes training and testing datasets to assess the efficacy of PSO-CatBoost in accurately forecasting the compressive strength the CFRP-CC. Every algorithm gets started with a predetermined set of values, known as hyperparameters, which determine the specific features of the algorithm before the training process begins. Getting to the point of optimal performance in machine learning algorithms necessitates the successful optimization of hyperparameters. Therefore, the PSO algorithm was employed to optimize the hyperparameters. Furthermore, the effectiveness of the PSO-CatBoost model in predicting the strength of CFRP-CC specimens was demonstrated by comparing the

Table 4
Summary of test results of CFRP-wrapped concrete.

No.	Author	No. of test	Fiber type	D (mm)	H (mm)	f`co (MPa)	C-Type (L,N,H)	E_f (GPa)	f_f (MPa)	t_f (mm)	No. of layers	ρf
1	Erdil et al. [40]	1	CFRP	150	300	11.1	L	230	3430	0.17	1	0.004
2	Ilki et al. [41]	12	CFRP	150	300	6.2	L	230	3430	0.17–0.99	1–6	0.004–0.027
3	Karantzikis et al. [42]	1	CFRP	200	35	12.1	L	230	3500	0.12	1	0.002
4	Pon et al. [43]	8	CFRP	150–600	300–1200	7.1–9.6	L	235	4410	0.22–0.33	2–3	0.002–0.009
5	Abdelrahman and El—Hacha [44]	1	CFRP	300	600	38.3	N	65	895	0.38	2	0.005
6	Aire et al. [45]	3	CFRP	150	300	42	N	240	3900	0.12–0.7	1–6	0.003–0.019
7	Akogbe et al. [46]	12	CFRP	100–300	200–600	21.7–26.5	N	242	3248	0.17–0.5	1–3	0.007
8	Al-Salloum [47]	2	CFRP	150	300	32.4–36.2	N	75	935	1.2	1	0.032
9	Benzaid et al. [48]	4	CFRP	160	320	25.93–49.46	N	238	4300	0.13–0.39	1–3	0.003–0.010
10	Berthet et al. [49]	27	CFRP	160	320	25–52	N	230	3200	0.11–1.32	1–4	0.003–0.011
11	Bisby et al. [50]	3	CFRP	150	300	34.4	N	231	4100	0.12	1	0.003
12	Bisby et al. [51]	3	CFRP	100	200	28	N	231	4100	0.12	1	0.005
13	Bouchelaghem et al. [52]	1	CFRP	160	320	26	N	55	750	0.52	1	0.013
14	Campione et al. [53]	1	CFRP	100	200	20.1	N	230	3430	0.17	2	0.007
15	Carey and Harries [54]	8	CFRP	152–254	305–762	32.1–38.9	N	25–250	875–3500	0.1–1.7	1–3	0.003–0.045
16	Chastre and Silva [55]	5	CFRP	150–250	750	35.2–38	N	226–241	3254–3711	0.33–0.5	2–3	0.006–0.013
17	Cui and Sheikh [56]	12	CFRP	152	305	45.6–48.1	N	85–241	816–3639	0.11–3	1–3	0.003–0.081
18	De Lorenzis et al. [57]	4	CFRP	120–150	240–300	38–43	N	91	1028	0.3–0.45	2–3	0.010–0.012
19	Demers and Neale [58]	4	CFRP	152	305	32.2–43.7	N	25	380	1–3	1–3	0.026–0.081
20	Dias da Silva and Santos [59]	3	CFRP	150	600	28.2	N	240	3700	0.11–0.33	1–3	0.003–0.009
21	Elsanadedy et al. [60]	6	CFRP	50–150	100–300	41.1–53.8	N	77	846	1–3	1–3	0.027–0.082
22	Erdil et al. [40]	1	CFRP	150	300	20.8	N	230	3430	0.17	1	0.004
23	Evans et al. [61]	1	CFRP	152	305	37.3	N	240	3800	0.23	1	0.006
24	Green et al. [62]	2	CFRP	152	305	46	N	22	237	1–2	1–2	0.026–0.053
25	Harmon and Slattery [63,64]	5	CFRP	51	102	41	N	235	3500	0.09–0.69	1–7	0.007–0.055
26	Harries and Kharel [64]	3	CFRP	152	305	32.1	N	16	174	1–3	1–3	0.026–0.081
27	Hosotani et al. [65]	1	CFRP	200	600	41.7	N	243	4227	0.44	1	0.009
28	Howie and Karbahari [66]	16	CFRP	152	305	38.6–42.5	N	71–227	755–3500	0.31–1.32	1–8	0.008–0.035
29	Ilki et al. [67,68]	5	CFRP	150	300	32	N	230	3430	0.17–0.83	1–5	0.004–0.022
30	Choudhury et al. [68]	5	CFRP	100–200	200–400	28.86–35.21	N	230	4900	0.12	1	0.002–0.005
31	Issa [69]	3	CFRP	150	300	23.6–23.9	N	231	4100	0.12	1	0.003
32	Issa et al. [70]	9	CFRP	150	300	30.5	N	230	4100	0.12–0.37	1–3	0.003–0.010
33	Jiang and Teng [15]	15	CFRP	152	305	37.7–47.6	N	241–260	2500	0.11–1.36	1–4	0.003–0.036
34	Jiang et al. [71]	24	CFRP	150	300	28.36–38.58	N	245	3922	0.17–0.5	1–3	0.004–0.013
35	Karabinis and Rousakis [72]	16	CFRP	200	320	35.7–38.5	N	240	3720	0.12–0.35	1–3	0.002–0.007
36	Karam and Tabbara [72]	2	CFRP	150	300	12.8	N	231	3650	0.12–0.24	1–2	0.003–0.006
37	Karbhari and Gao [32]	3	CFRP	152	305	38.4	N	77–138	1047–1352	0.66–1.32	2–4	0.017–0.035
38	Kono et al. [73]	21	CFRP	100	200	32.3–34.8	N	235	3820	0.17–0.5	1–3	0.007–0.020
39	Lam and Teng [74]	12	CFRP	152	305	34.3–35.9	N	251	2500	0.17–0.5	1–3	0.004–0.013
40	Lam et al. [75]	6	CFRP	153	305	38.9–41.1	N	251	2500	0.17–0.33	1–2	0.004–0.009
41	Lee et al. [76]	5	CFRP	150	300	36.2	N	250	4510	0.11–0.55	1–5	0.003–0.015
42	Li et al. [77]	2	CFRP	300	600	16.68	N	231	4120	0.11–0.22	1–2	0.001–0.003
43	Li et al. [78]	6	CFRP	150	300	25.5–49.6	N	242	4338	0.17	1	0.004
44	Liang et al. [64]	12	CFRP	100–300	200–600	22.7–25.9	N	245	3248	0.17–0.5	1–3	0.007
45	Lin and Li [79]	27	CFRP	100–150	200–300	17.7–25.9	N	232	4170	0.14–0.41	1–3	0.004–0.017
46	Mandal et al. [31]	3	CFRP	102	200	30.7–54.5	N	47	784	0.8	1	0.032
47	Matthys et al. [80]	3	CFRP	150	300	34.9	N	240	2600	0.12	1	0.003
48	Micelli et al. [81]	1	CFRP	102	204	37	N	227	3790	0.16	1	0.006
49	Miyauchi et al. [82]	10	CFRP	100–150	200–300	31.2–51.9	N	231	3481	0.11–0.33	1–3	0.003–0.013
50	Miyauchi et al. [83]	6	CFRP	100–150	200–300	23.6–26.3	N	231	3481	0.11–0.33	1–3	0.003–0.013
51	Modarelli et al. [84]	2	CFRP	150	300	28.35–38.24	N	221	3070	0.17	1	0.004

(*continued on next page*)

Table 4 (*continued*)

No.	Author	No. of test	Fiber type	D (mm)	H (mm)	f'co (MPa)	C-Type (L,N,H)	E_f (GPa)	f_f (MPa)	t_f (mm)	No. of layers	ρf
52	Moretti and Arvanitopoulos [85]	15	CFRP	100–152	200–305	17.6–20	N	230	3910	0.13–0.26	1–2	0.003–0.007
53	Ongpeng [86]	2	CFRP	180	500	27	N	231	3650	0.13–0.26	1–2	0.003–0.006
54	Owen [87]	8	CFRP	102–152	203–305	47.9–53	N	262	4200	0.17–1.32	1–8	0.006–0.052
55	Pessiki et al. [14]	2	CFRP	152	610	26.2	N	38	580	1–2	1–2	0.026–0.053
56	Picher et al. [88]	1	CFRP	152	304	39.7	N	83	1266	0.9	2	0.024
57	Piekarczyk et al. [89]	2	CFRP	47	112	55	N	110–113	1150–1420	0.51–0.82	2	0.044–0.071
58	Purba and Mufti [90]	1	CFRP	191	788	27.1	N	231	3483	0.22	2	0.005
59	Rochette and Labossiére [91]	3	CFRP	100	200	42	N	83	1265	0.6	2	0.024
60	Rousakis et al. [92]	6	CFRP	150	300	20.4–49.2	N	234	4493	0.17–0.51	1–3	0.005–0.014
61	Saenz and Pantelides [93]	4	CFRP	152	304	40.3–47.5	N	87	1220	1–2	1–2	0.026–0.053
62	Santarosa et al. [94]	3	CFRP	150	300	15.3–28.1	N	230	3400	0.11–0.22	1–2	0.003–0.006
63	Shahawy et al. [17]	9	CFRP	153	305	19.4–49	N	83	2275	0.36–1.25	1–5	0.009–0.033
64	Shehata et al. [95]	8	CFRP	150–225	300–450	25.6–34	N	235	3550	0.17–0.33	1–2	0.003–0.009
65	Smith et al. [96]	4	CFRP	250	500	35	N	211	3182	0.26	2	0.004
66	Song et al. [97]	12	CFRP	100–150	300–450	22.4–40.9	N	237	4073	0.13–0.39	1–3	0.003–0.016
67	Stanton and Owen [98]	5	CFRP	153	305	49	N	238–262	4200	0.17–1.32	1–8	0.004–0.035
68	Suter and Pinzelli [99]	1	CFRP	150	300	44.7	N	240	3800	0.23	2	0.006
69	Tamuzs et al. [100]	4	CFRP	150	300	20.8–48.8	N	231	2390	0.34	2	0.009
70	Thériault et al. [101]	3	CFRP	51–304	102–608	18–37	N	230	3481	0.17–0.66	1–4	0.009–0.013
71	Touhari and Mitiche-Kettab [102]	18	CFRP	160	320	24–41.6	N	34	403	1–3	1–3	0.025–0.076
72	Toutanji and Deng [103]	3	CFRP	76	152	30.9–31.8	N	73–231	1519–3485	0.22–0.57	2–5	0.012–0.030
73	Valdmanis et al. [104]	6	CFRP	150	300	40–44.3	N	201–236	1906–2661	0.17–0.51	1–3	0.005–0.014
74	Vincent and Ozbakkaloglu [105]	6	CFRP	152	305	35.5–38	N	240	3800	0.12–0.23	1–2	0.003–0.006
75	Wang and Cheong [106]	2	CFRP	200	600	27.9	N	235	4400	0.36	2	0.007
76	Wang and Wu [107]	12	CFRP	150	300	30.9–52.1	N	219–226	3788–4364	0.17–0.33	1–2	0.004–0.009
77	Wang et al. [108].	4	CFRP	204–305	612–915	24.5	N	240–244	4340–4344	0.17–0.33	1–2	0.002–0.007
78	Watanabe et al. [109]	3	CFRP	100	200	30.2	N	225	2658–2873	0.17–0.67	1–4	0.007–0.027
79	Wu and Jiang [110]	38	CFRP	150	300	20.6–36.7	N	242–254	4192–4441	0.17–0.67	1–4	0.004–0.018
80	Wu et al. [111]	4	CFRP	150	300	23–23.1	N	243	4234	0.17–0.33	1–2	0.004–0.009
81	Xiao and Wu [112]	27	CFRP	152	305	33.7–55.2	N	105	1577	0.38–1.14	1–3	0.010–0.030
82	Yan et al. [113]	1	CFRP	305	610	15	N	87	1220	1	3	0.013
83	Youseff [114]	2	CFRP	406	812	38.3–45.6	N	105	1246	2.34	2	0.023
84	Youssef et al. [115]	19	CFRP	152–406	305–813	29.4–44.6	N	104	1246	1.17–5.84	2–9	0.012–0.062
85	Zhang et al. [116]	1	CFRP	150	300	34.3	N	91	753	1	1	0.027
86	Wang et al. [117]	2	CFRP	100	200	32	N	105	1674	1.18	1	0.048
87	Toutanji [16]	1	CFRP	76	305	30.93	N	231	3485	0.22	2	0.012
88	Al-Salloum [118, 119]	2	CFRP	150	300	32.4–36.23	N	75	935	1.2	1	0.032
89	De Lorenzis et al. [57]	1	CFRP	55	110	43	N	91	1028	0.15	1	0.011
90	Ilki and Kumbasar [120]	5	CFRP	150	300	32	N	230	3430	0.17–0.83	1–5	0.004–0.022
91	Toutanji and Balaguru [121]	1	CFRP	76	305	31.8	N	228	3485	0.22	2	0.012
92	Lin and Chen [122]	4	CFRP	120	240	32.7	N	158	770	0.5–1	1–2	0.017–0.034
93	Bullo [123]	6	HM_CFRP	150	300	32.54	N	390	3000	0.17–0.5	1–3	0.004–0.013
94	Cui and Sheikh [56]	6	HM CFRP	152	305	45.7	N	436	3314	0.16–0.49	1–3	0.004–0.013
95	Dias da Silva and Santos [59]	3	HM_CFRP	150	600	28.2	N	390	3000	0.17–0.5	1–3	0.005–0.13
96	Hosotani et al. [65]	1	HM_CFRP	200	600	41.7	N	439	3972	0.68	1	0.014
97	Rousakis and Tepfers [124]	20	HM_CFRP	150	300	25.2–51.8	N	377	4410	0.17–0.85	1–5	0.005–0.023
98	Matthys et al. [80]	2	UHM_CFRP	150	300	34.9	N	420–640	1100–2650	0.24	1–2	0.006
99	Suter and Pinzelli [99]	1	UHM_CFRP	150	300	44.7	N	640	2650	0.38	3	0.010

(*continued on next page*)

Table 4 (*continued*)

No.	Author	No. of test	Fiber type	D (mm)	H (mm)	f'co (MPa)	C-Type (L,N,H)	E_f (GPa)	f_f (MPa)	t_f (mm)	No. of layers	ρf
100	Toutanji and Deng [103]	1	HM_CFRP	76	152	30.9	N	373	2940	0.33	3	0.017
101	Watanabe et al. [109]	3	UHM_CFRP	100	200	30.2	N	576–629	1285–1824	0.14–0.42	1–3	0.006–0.017
102	Wu et al. [111]	3	UHM_CFRP	150	300	23–23.1	N	563	2544	0.29	2	0.008
103	Toutanji [16]	1	HM_CFRP	76	305	30.93	N	373	2940	0.33	2	0.017
104	Toutanji and Balaguru [121]	1	HM_CFRP	76	305	31.8	N	373	2940	0.33	2	0.017
105	Aire et al. [45]	5	CFRP	150	300	69	H	240	3900	0.12–1.4	1–12	0.003–0.038
106	Benzaid et al. [48]	2	CFRP	160	320	61.81	H	238	4300	0.13–0.39	1–3	0.003–0.010
107	Berthet et al. [49]	6	CFRP	70	140	112.6–169.7	H	230	3200	0.33–0.99	3–9	0.019–0.057
108	Chikh et al. [119]	2	CFRP	160	320	61.8	H	238	4300	0.13–0.39	1–3	0.003–0.010
109	Cui and Sheikh [56]	20	CFRP	152	305	79.9–111.8	H	85–241	816–3639	0.11–3	1–5	0.003–0.081
110	Green [125]	1	CFRP	152	305	59	H	70	881	1	1	0.026
111	Harmon and Slattery [63]	3	CFRP	51	102	103	H	235	3500	0.18–0.69	1–4	0.014–0.055
112	Li et al. [78]	2	CFRP	150	300	60.5	H	242	4338	0.17	1	0.004
113	Mandal and Fam [126]	6	CFRP	100	200	67.03–80.6	H	47	784	0.8	4	0.032
114	Miyauchi et al. [83]	2	CFRP	100	200	109.5	H	231	3481	0.11–0.22	1–2	0.004–0.009
115	Owen [87]	3	CFRP	298	610	58.1	H	238	4200	1.32	2–7	0.018
116	Shehata et al. [95]	2	CFRP	150	300	61.7	H	235	3550	0.17–0.33	1–3	0.004–0.009
117	Touhari and Mitiche-Kettab [102]	9	CFRP	160	320	61.5	H	34	403	1–3	1–3	0.025–0.076
118	Valdmanis et al. [104]	3	CFRP	150	300	61.6	H	201–236	1906–2661	0.17–0.51	1–3	0.005–0.014
119	Xiao et al. [127].	12	CFRP	152	305	70.8–111.6	H	238	2738	0.34–1.7	2–10	0.009–0.045
120	Vincent and Ozbakkaloglu [105]	11	CFRP	152	305	62.4–65.8	H	240	3800	0.12–0.47	1–4	0.003–0.012
121	Ozbakkaloglu and Vincent [128]	1	CFRP	152	305	108	H	240	3800	0.47	4	0.012
122	Ozbakkaloglu and Vincent [128]	1	CFRP	152	305	112	H	240	3800	0.59	5	0.015
123	Ozbakkaloglu and Vincent [56]	1	CFRP	152	305	110	H	240	3800	0.7	6	0.019
124	Cui and Sheikh [56]	10	HM _CFRP	152	305	85.6–111.8	H	436	3314	0.16–0.82	1–5	0.004–0.022
125	Rousakis and Tepfers [124]	14	HM _CFRP	150	300	56.9–82.1	H	377	4410	0.17–0.51	1–3	0.005–0.014
126	Vincent and Ozbakkaloglu [105]	33	HM _CFRP	100–152.5	300–305	73–121.2	H	118–436	2060–3314	0.16–1.2	1–6	0.009–0.035

other six models mentioned in Section 2. Table 6 displays a comprehensive set of optimized hyperparameters utilized in the process of training the model. The model's performance was assessed using several metrics in the following subsection. All predictive model applications were run on a personal computer equipped with an Apple M2 Max processor, 96GB of RAM, and utilizing the macOS Ventura operating system.

5.1. Performance measures

To evaluate the accuracy of the developed model and compare it with available analytical models in the literature, several statistical indices were employed, such as coefficient of determination (R^2), mean square error (MSE), root mean square error (RMSE), mean absolute error (MAE), and residual standard error (RSE).

5.1.1. Residual error

Regardless of how well a model predicts the target value, there are always random errors. The difference between the predicted and observed values is often called the "residual" or "error," and one of the goals of training a model is to minimize this difference.

$$e = x_{Experimental} - x_{Predicted} \tag{9}$$

where e is the residual error defined as the difference between the experimental data and the predicted value by the model, x_{exp} is the measured value in the experiment, x_{mod} is the value predicted by the model,

5.1.2. Coefficient of determination

The coefficient of determination can take a value between 0 and 1, quantifying how accurately a model predicts the result. The coefficient of determination is calculated using Eq. (10).

$$R^2 = 1 - \frac{\sum_{i=1}^{N}\left(x_{exp,i} - x_{mod,i}\right)^2}{\sum_{i=1}^{N}\left(x_{exp,i} - \bar{x}\right)^2} \tag{10}$$

where x_{exp} is the measured value in the experiment, x_{mod} is the value predicted by the model, $\bar{x}$ is the average of x_{exp}, and N is the total number of test data.

5.1.3. Mean squared error

The mean squared error is the squared average value of the difference between the experimental data and the predicted values by the model and can be calculated according to Eq. (11).

$$MSE = \frac{1}{N}\sum_{i=1}^{N}\left(x_{exp,i} - x_{mod,i}\right)^2 \tag{11}$$

where x_{exp} is the measured value in the experiment, x_{mod} is the value

Table 5
Summary of test results of CFRP tube-encased concrete.

No.	Author	No. of test	Fiber Type	D (mm)	H (mm)	f'co (MPa)	C-Type (L,N, H)	E_f (GPa)	f_f (MPa)	t_f (mm)	No. of Layers	ρf
127	Hong and Kim [129]	2	CFRP	300	600	17.5	N	137	2058	2–3	2–3	0.027–0.040
128	Karantzikis et al. [42]	1	CFRP	200	350	12.1	L	230	3500	0.12	1	0.002
129	Lim and Ozbakkaloglu [130]	6	CFRP	152.5	305	29.6–49.6	N	236	4152	0.17–0.33	1–2	0.004–0.009
130	Matthys et al. [80]	2	HM_CFRP	150	300	34.9	N	200–420	1100–2600	0.12–0.24	1–2	0.003–0.006
131	Ozbakkaloglu and Vincent [131]	14	CFRP	74–302	152–600	34.6–55	N	240	3800	0.12–0.47	1–4	0.006–0.013
132	Ozbakkaloglu and Vincent [131]	4	UHM CFRP	100–152	200–305	35.4–36.3	N	640	2650	0.19	2	0.005–0.008
133	Saafi et al. [132].	3	HM_CFRP	152	435	35	N	367–415	3300–3700	0.11–0.55	1–5	0.003–0.015
134	Vincent and Ozbakkaloglu [133]	21	CFRP	152	305	52	N	230	4370	0.33	3	0.009
135	Lim and Ozbakkaloglu [134]	6	CFRP	152	305	29.6–49.6	N	236	4152	0.17–0.33	1–2	0.004–0.009
136	Lim and Ozbakkalaglu [130]	6	UHM_CFRP	152.5	305	74.1–98	H	236	4152	0.5–0.66	2–3	0.013–0.0170
137	Ozbakkaloglu and Vincent [131]	6	CFRP	152	305	55.6–59	H	640	2650	0.19–0.38	1–2	0.005–0.010
138	Vincent and Ozbakkaloglu [133]	12	CFRP	152	305	84.7	H	230	4370	0.67	6	0.018
139	Lim and Ozbakkaloglu [134]	6	CFRP	152	305	74.1–98	H	236	4152	0.5–0.66	3–4	0.013–0.017
140	Vincent and Ozbakkaloglu [105]	22	CFRP	152	305	59–102.5	H	240	3800	0.12–0.59	1–5	0.009–0.015
141	Ozbakkaloglu and Akin [128]	1	CFRP	152	305	100	H	240	3800	0.47	4	0.012
142	Vincent and Ozbakkaloglu [105]	2	CFRP	152	305	97.5–102.5	H	240	3800	0.47–0.7	4–7	0.012–0.019
143	Ozbakkaloglu and Akin [128]	1	CFRP	152	305	94	H	240	3800	0.7	6	0.019
144	Vincent and Ozbakkaloglu [105]	1	CFRP	152	305	93	H	240	3800	0.7	4	0.019

PSO-CatBoost Algorithm

Initialize *the swarm particles with random positions within the search space (hyperparameters for CatBoost).*
For *each particle*
Initialize particle position Xi randomly within the search space
Initialize particle velocity Vi randomly within a specified range
Evaluate the fitness of each particle by training CatBoost and measuring its performance
Initialize *the global best position G with the best particle*
While *stopping criteria are not met:*
For *each particle*
Update *the particle position*
Update *the particle velocity*
Evaluate *the fitness of each particle by training CatBoost and measuring its performance*
If *the fitness of each particle is better than its personal best:*
Update personal best position
If *the fitness of each particle is better than the global best:*
Update global best position
Use *the global best position as the final solution*
End while
Return best hyperparameters and fitness

Fig. 5. Pseudo code of PSO-CatBoost.

predicted by the model, and N is the total number of test data points.

5.1.4. Root mean squared error

Another way to evaluate the accuracy of a fit is to calculate the root mean squared error according to Eq. (12). The RMSE is a measure that demonstrates the mean distance between the values predicted by the model and the experimental values from the dataset.

$$RMSE = \sqrt{\frac{\sum_{i=1}^{N}\left(x_{exp,i} - x_{mod,i}\right)^2}{N}} \tag{12}$$

5.1.5. Mean absolute error

The mean absolute error is the average value of the absolute difference between the experimental data and the predicted values by the model and can be calculated according to Eq. (13).

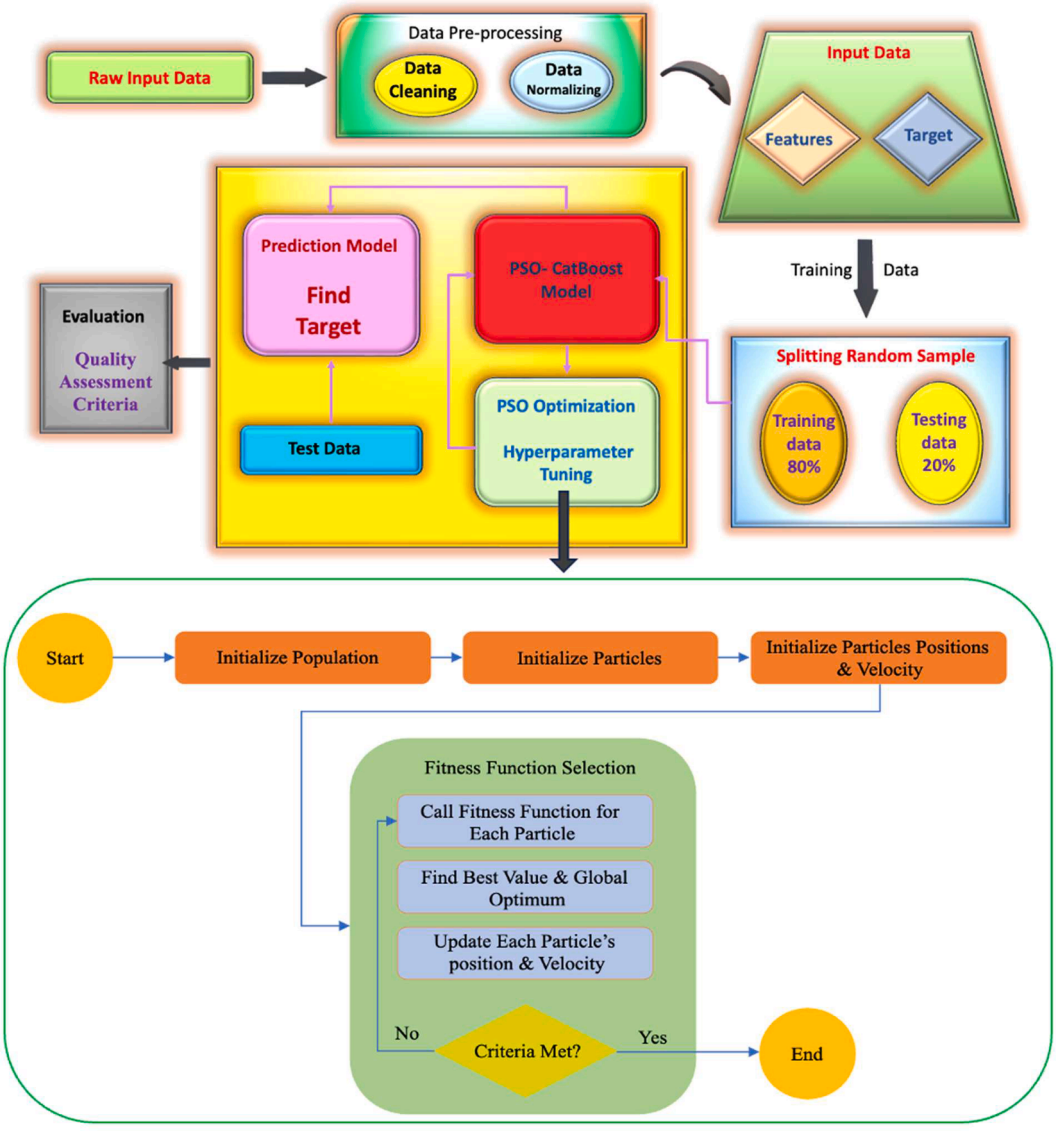

Fig. 6. The architectural detail PSO-CatBoost model.

Table 6
Optimum hyperparameters value for PSO—CatBoost model.

Algorithm	Hyperparameters	Optimum value
PSO	Local coefficient (c_1)	*0.5*
	Global coefficient (c_2)	*0.3*
	Inertia coefficient (w)	*0.9*
	Maximum iteration count (max_{iter})	*500*
	Population/swarm size (s)	*10*
CatBoost	Depth	*4.046*
	Learning rate	*0.1*
	L2-regularization	*1.959*

$$MAE = \frac{1}{N}\sum_{i=1}^{N}\left|x_{exp,i} - x_{mod,i}\right| \tag{13}$$

where x_{exp} is the measured value in the experiment, x_{mod} is the value predicted by the model, $\overline{x}$ is the average of x_{exp}, and N is the total number of test data.

5.2. Interpretation of model results

Over the past few years, most ML techniques for regression and classification problems have considerably improved their effectiveness in real-world scenarios. These advancements have been made possible by recent advances in computer processing power. While machine learning is increasingly integrated into daily life, its use is still primarily limited to individuals with specialized knowledge. The technical complexity of machine learning, which relies on advanced mathematics, statistics, and coding skills, presents a significant barrier to entry for non-experts A traditional ML setup in its most basic version entails several crucial steps, including modifying data, model selection, model building, model examination, and deploying the model. In the ML setup, the critical stage of hyperparameter tuning is an essential part of the model generation process. When machine learning algorithms have had their hyperparameters effectively optimized, hardly ever will they be able to achieve the maximum level of performance possible. In this study, the CatBoost algorithm with PSO was developed for the dataset.

Additionally, other models are put side by side with this new model to demonstrate the model's effectiveness for the current dataset. The data used for the models were derived from the experiment results presented in Tables 6 and 7. This model was trained using a distribution

Table 7
Performance metric results for the employed method.

Data	R^2	MSE	MAE	RMSE
Train	0.9898	0.0008	0.0219	0.0290
Test	0.9572	0.0026	0.0373	0.0514
All	0.9847	0.0012	0.0250	0.0347

of 80 % of the data, while 20 % of the data was set aside for testing. Input parameters that were provided to the model included the diameter of the compression member (D), the height of the compression member (H), the compressive strength of unconfined concrete (f'_{co}), FRP reinforcement ratio (ρ_f), the tensile modulus of elasticity (E_f), the ultimate tensile strength of FRP (f_f), nominal thickness of FRP reinforcement (t_f) and number of FRP layers (*Layers*). On the other hand, the output parameters concentrated on the compressive strength of the specimen after confinement. The quality evaluation criteria presented earlier are used for evaluating the model's performance.

The correlations between the characteristics were analyzed using the Spearman correlation technique. The Spearman correlation captures not only linear but also non-linear correlations between variables, in contrast to the Pearson correlation, which only considers linear ones.

Spearman correlation coefficients (s) are shown in Fig. 7 for a variety of input features. There is a strong positive correlation between the thickness of FRP reinforcement (t_f) and FRP reinforcement ratio (ρ_f) of (s = 0.94) as well as the diameter (D) and height of specimen (H) (s = 0.93). It makes it natural that this would be the case because the strength of a specimen depends on its specific geometry. The number of layers (*Layers*) has moderate correlations with the thickness of FRP reinforcement (t_f) ($s = 0.68$) as well as the FRP reinforcement ratio (ρ_f) ($s = 0.65$). Different charts show a comparison and analysis of the data. These findings include the coefficient of determination, mean squared error, and root mean squared error.

A coefficient of determination (R^2) greater than 0.95 indicates excellent predictive abilities, whereas values falling between 0.75 and 0.95 indicate reliable and accurate model predictions. On the contrary, values that are lower than 0.60 indicate below-average performance. Table 7 contains the performance metrics of the PSO-CatBoost. The PSO-CatBoost model achieved R^2 scores of 0.9898 and 0.9572 in the training and testing phases, respectively, which is worth mentioning. The findings presented in this study clearly demonstrate that the model under investigation can accurately forecast the compressive strength of CFRP-CC. In addition, the PSO-CatBoost model showed comparatively lower error values throughout both the training and testing phases based on MSE, MAE, and RMSE.

Fig. 8-a displays the PSO-CatBoost model prediction for train data. Based on this figure, the training data and the prediction model exhibit exceptional congruence, demonstrating the model's effectiveness. This high degree of overlap indicates the model's ability to accurately reflect and predict the underlying patterns in the training data. The error margins for the training data indicate a high level of accuracy, affirming that the model performs exceptionally well. Notably, most errors are less than 0.025, further attesting to the model's precision (See Fig. 8-b). A high correlation between the training data's input features and output variables signifies a robust association. This measures the model's ability to effectively learn and internalize the patterns and correlations in the data during the training phase. This typically results in better predictive performance when the model encounters new data. By improving the precision and robustness of its predictions, the model becomes more functional and valuable for practical applications. The correlation patterns in the training data for this model are depicted in Fig. 8-c. The model exhibits a high R-squared value of 0.9898, signifying a strong relationship between the independent and dependent variables in the training dataset, indicating the model's effectiveness.

The test data in ML is referred to as the subset of the dataset that is used to assess the performance of the produced model after it has been trained. This dataset has been preserved apart from the training data to evaluate the model's ability to handle novel data reasonably. When it comes to machine learning, the findings from test data typically provide metrics that show the performance and resilience of the model.

Fig. 9-a shows the predicted and observed values for the test data. When the test data closely matches the target or desired output, it demonstrates that the model has been effectively trained and is able to generalize well to unseen data. This is a desirable characteristic, as it indicates that the model is not overfitting to the training data and is able to make accurate predictions on new data. The error between the observed and predicted value for test data is shown in Fig. 9-b. In ML, the error in predicted data is typically evaluated by comparing the predicted outcomes from the model to the actual (or target) outcomes. Based on Fig. 9-c, an R-squared value of 0.9572 for the test data suggests a strong correlation between the model's predictions and the actual outcomes. In simpler terms, the model is able to explain about 95.72 % of the variation in the data one is trying to predict, which is typically considered a high level of accuracy.

All available data was utilized in the recent testing of the predictive model. In the further assessment of the model's performance, a scatter

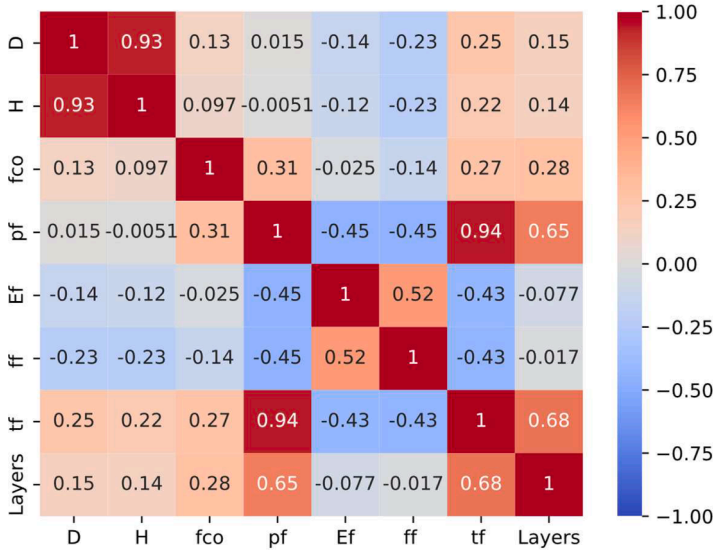

Fig. 7. Heatmap for the correlation coefficient between variables.

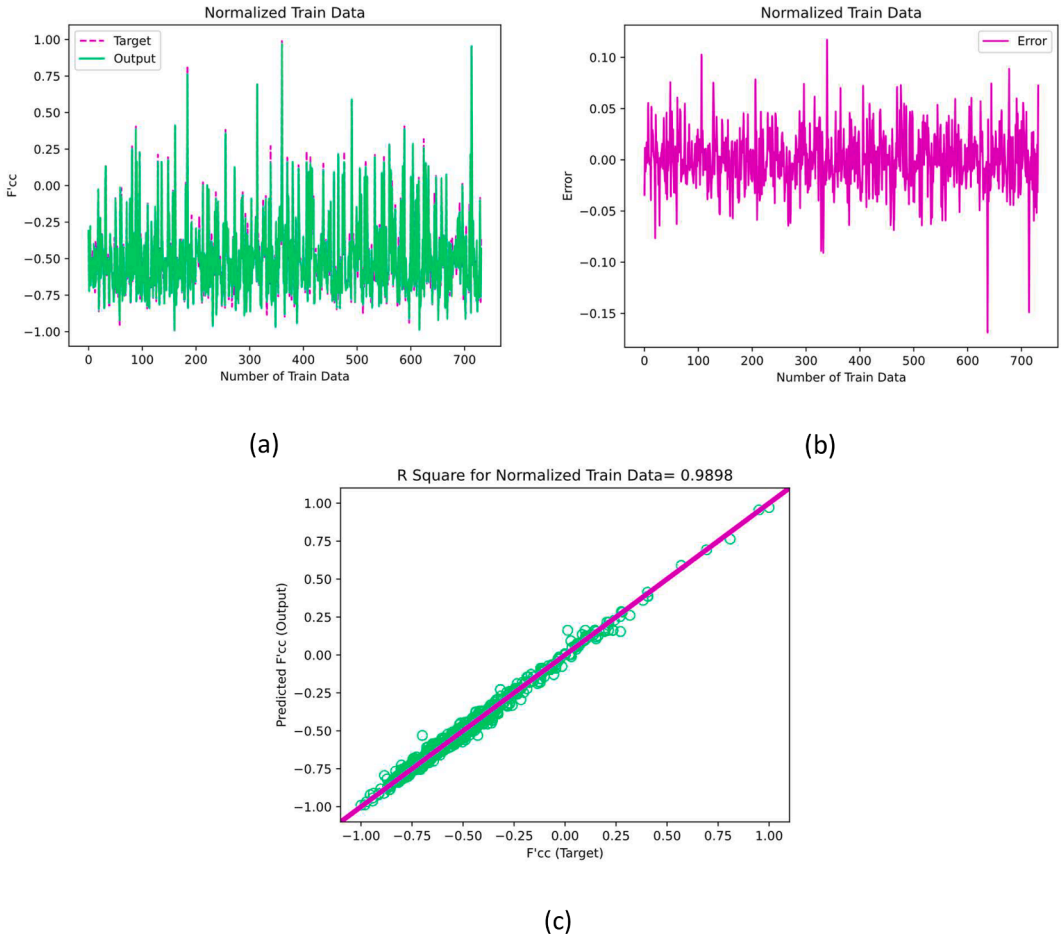

Fig. 8. Estimator result analysis of compressive strength for train data.

plot was created to visualize the differences between the predicted and target values, as depicted in Fig. 10-a. The scatter plot, as shown in Fig. 10-b, allows us to observe patterns in the model's residuals (the differences between predicted and actual values). Patterns in these residuals can reveal systematic under- or over-estimations by the model. According to Fig. 10-c, the model exhibited exceptional performance, producing an R-squared value of 0.9847. This value suggests that approximately 98.47 % of the variance in the dependent variable can be explained by the proposed model, an impressive achievement that signifies the ability of the model to predict the target variable based on the input features accurately. Further to this numerical evaluation, the performance of the model was visualized by plotting the predicted values against the actual ones (see Fig. 10-c). Ideally, this plot would depict a straight line following the equation $y = x$, where every predicted value exactly matches its corresponding actual value. In our test, the line of correlation very closely resembled this ideal scenario, indicating a high degree of accuracy in the predictions. The quantitative (R-squared value) and qualitative (correlation plot) results prove the model's robust predictive performance. The near-perfect alignment with the $y = x$ line in the plot further reinforces the reliability and precision of the predictions generated by the model.

The findings demonstrated that by utilizing CatBoost in conjunction with the PSO algorithm, the accuracy of estimating the compressive strength of CFRP-CC can be significantly improved. The suggested model can be readily applied to assess the compressive strength of CFRP-CC in a straightforward manner. The inclusion of the mean (μ) and standard deviation (σ) in Fig. 11 provides additional information about the distribution of the prediction errors. The figure and the Kernel Density Estimation (KDE) curve and histogram provide a visual representation of the distribution of prediction errors. Combining the graphical representation with the mean and standard deviation (SD) values allows one to evaluate the overall quality of the model's predictions and obtain insights into its performance and reliability. If the mean is close to zero and the sigma is relatively small, it suggests that the model's predictions are centered around the true values with low variability. The mean, denoted by μ, is approximately 0.00023, suggesting that the prediction errors are, on average, very close to zero. The standard deviation, denoted by σ, is approximately 0.05141, indicating the extent of dispersion or variability in the prediction errors around the mean.

Accroding to Fig. 12, a comparison of the proposed model with Mandal et al. [31], Karbhari et al. [32], Reza et al. [34], Realfonzo and Napoli [35] and Vintzileou and Panagiotidou [36] which illustrates a comparative visual analysis of six predictive models' performance using scatter plots for the target versus predicted f'_{cc}. Lillistone and Jolly [33] and Mandal et al. [31] show moderate dispersion of data points, indicating reasonable predictive accuracy with some variance, especially at the extremes of the f'_{cc} range. Karbhari et al. [32], Reza et al. [34], Realfonzo and Napoli [35] and Vintzileou and Panagiotidou [36] exhibit a tighter clustering of points along the unity line, especially in the mid-range, though accuracy diminishes at the lower and higher ends of the target values. Notably, the present work scatter plot presents a remarkable alignment of data points with the line of perfect prediction across the full spectrum of f'_{cc} values, suggesting that the current model significantly outperforms its predecessors in terms of predictive precision, as indicated by the minimal deviation from the unity line.

Fig. 13 provides more information on the relevant RMSE, MSE, and MAE values. According to the results, the PSO-CatBoost predicts quite

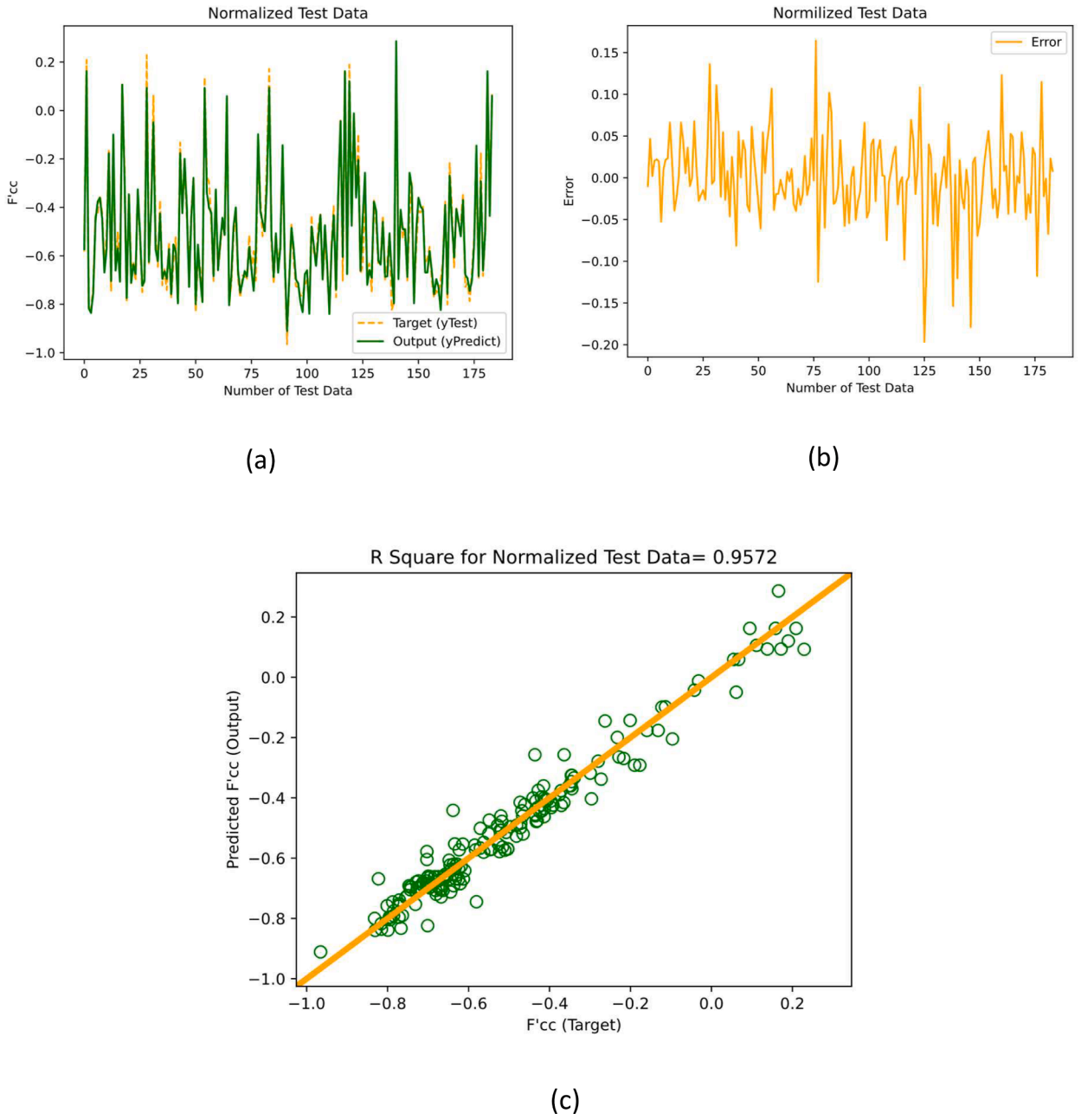

Fig. 9. Estimator result analysis of compressive strength for test data.

accurately and PSO-CatBoost clearly outperforms other strategies. The proposed model obtains an RMSE of 0.0347, an MSE of 0.0012, and an MAE of 0.0250 based on the performance metric values. These values are noticeably lower than those for the other empirical equations.

For a clearer understanding of how the R-squared values compare to other approaches, see Fig. 14. The bar chart illustrates the comparative performance of different predictive models using numerical error metrics: RMSE, MAE, and MSE. The present work shows exceptionally low RMSE (0.0347), MAE (0.025), and MSE (0.0012), indicating it has the highest predictive accuracy among the evaluated models. Lillistone and Jolly have the highest RMSE (0.0532) and MAE (0.1742), and Mandal et al. have the highest MSE (0.2358), reflecting less precision in their predictions. The remaining models, Vintzileou and Panagiotidou, Realfozo and Napoli, Reza et al., and Karbhari and Gao, show intermediate values with RMSEs ranging from 0.0246 to 0.0265, MAEs from 0.123 to 0.134, and MSEs from 0.1287 to 0.1628. These numbers are critical for understanding the exact quantitative differences in model performance, with the present work model being quantitatively superior.

The correlation coefficients, root mean squared deviation, and standard deviation of the patterns utilized in this study are all represented graphically in the Taylor diagram. The Taylor diagram for the patterns is shown in Fig. 15. According to the results, the proposed model performs better than traditional models in most cases when evaluating the compressive strength of CFRP-CC because it has a more significant correlation coefficient, minor standard deviation, and lower RMSE.

In the initial methodology adopted, the performance of the PSO-Catboost model was assessed against established prediction formulas utilizing the entire dataset, including the training data. This approach raised potential concerns regarding overestimating the model's predictive accuracy, as the evaluation was conducted on data previously encountered during the training phase. Such a method of evaluation risked masking the actual generalization capacity of the model on novel, unseen datasets.

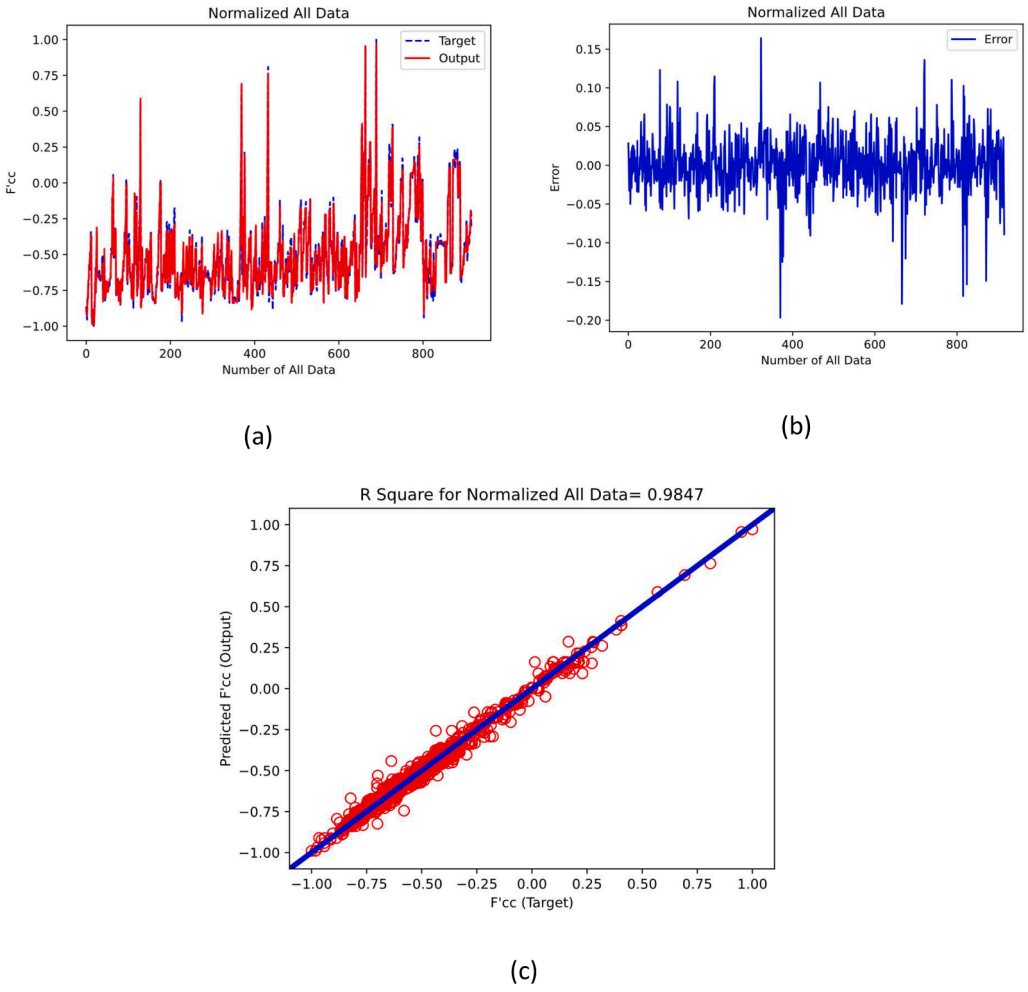

Fig. 10. Estimator result analysis of compressive strength for all data.

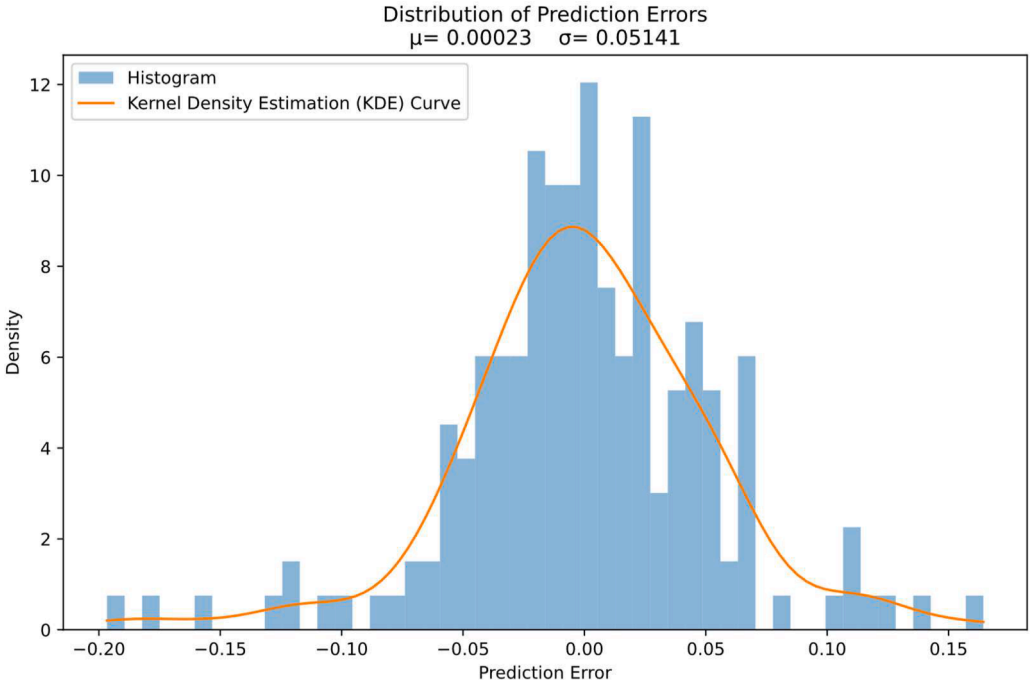

Fig. 11. Distribution of prediction error for model.

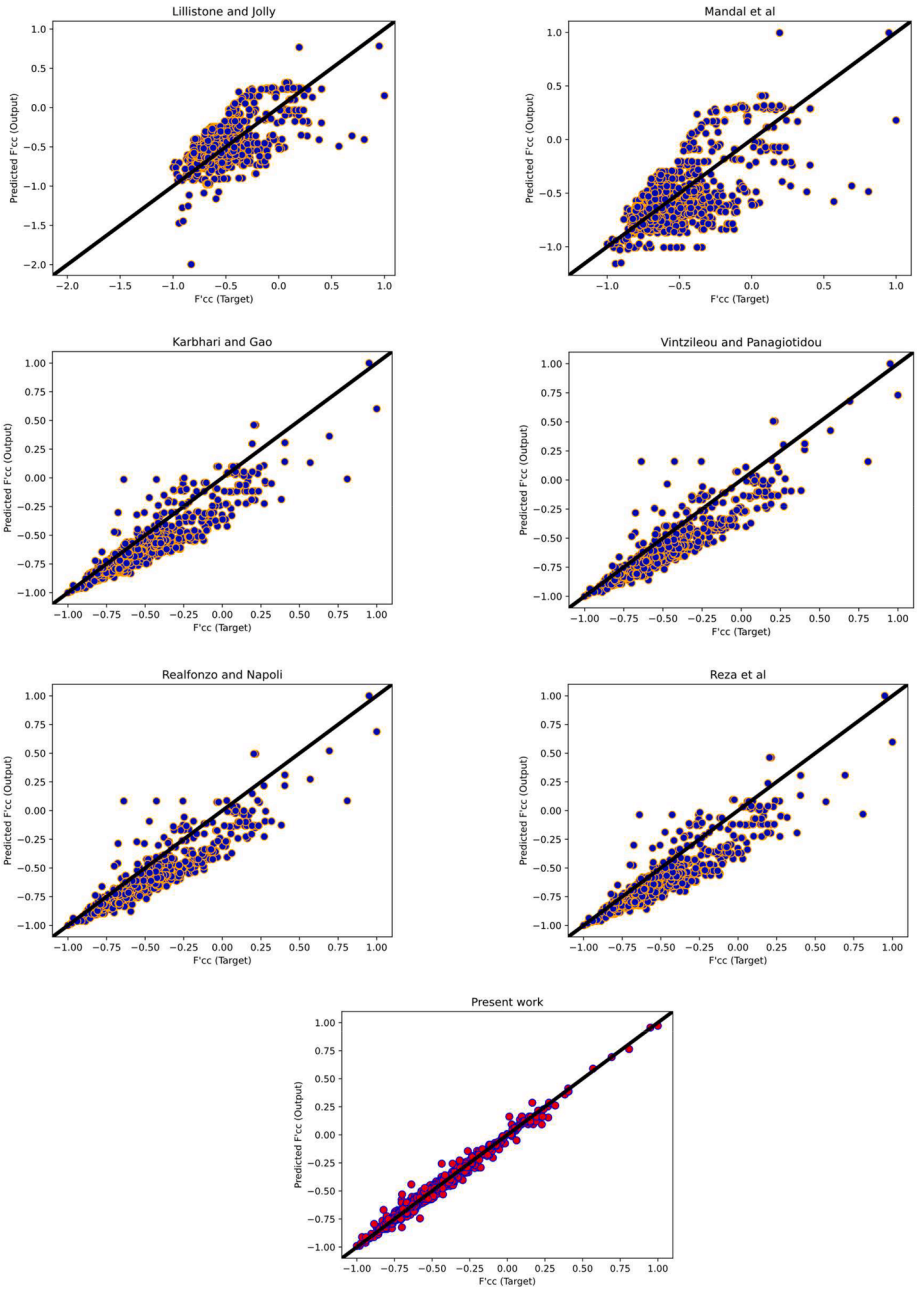

Fig. 12. Comparison of present work with other empirical methods.

In response to these concerns and to align with standard machine learning practices, the evaluation strategy was revised, acknowledging the segregation of the dataset into two discrete subsets: the training set and the testing set. In the training phase, the development and training of the Catboost model were confined exclusively to the training set, facilitating the learning of dataset-specific patterns without any overlap with the testing set. A critical element of the revised methodology is the testing phase, wherein the model's performance is solely evaluated on the testing set, consisting of data points that the model had not previously encountered. This ensures that the derived performance metrics indicate the model's ability to generalize new data. Moreover, comparing the Catboost model with existing prediction formulas has been restricted solely to the testing set, thereby ensuring a fair and unbiased comparison by evaluating each model's performance on data not included in their training set.

Fig. 16 assesses the performance of various predictive models (present work, Mandal et al., Lillistone and Jolly, Karbhari and Gao, Reza et al., Realfonzo and Napoli, and Vintzileou and Panagiotidou) against expected results (Ex) on a test dataset, focusing on three critical statistical error metrics: MSE, RMSE, and MAE. The present work model demonstrates exceptional precision, with the lowest MSE (0.0012), RMSE (0.0347), and MAE (0.0250), indicative of its predictions being highly consistent with the actual values. On the other hand, Mandal et al. and Lilliston and Jolly exhibit higher errors, especially in MSE and RMSE, denoting less precise predictions. Meanwhile, models Karbhari and Gao, Reza et al., Realfonzo and Napoli, and Vintzileou and Panagiotidou show intermediate error values, with Karbhari and Gao slightly outperforming the models' relative performance, highlighting the present work's efficacy performance of the models, highlighting the efficacy of the present work in the context of the test dataset. This chart effectively expresses the predictive accuracy of each model on the test dataset, with the present work model's results suggesting a solid alignment with the expected data and highlighting a need for improvement in the other models.

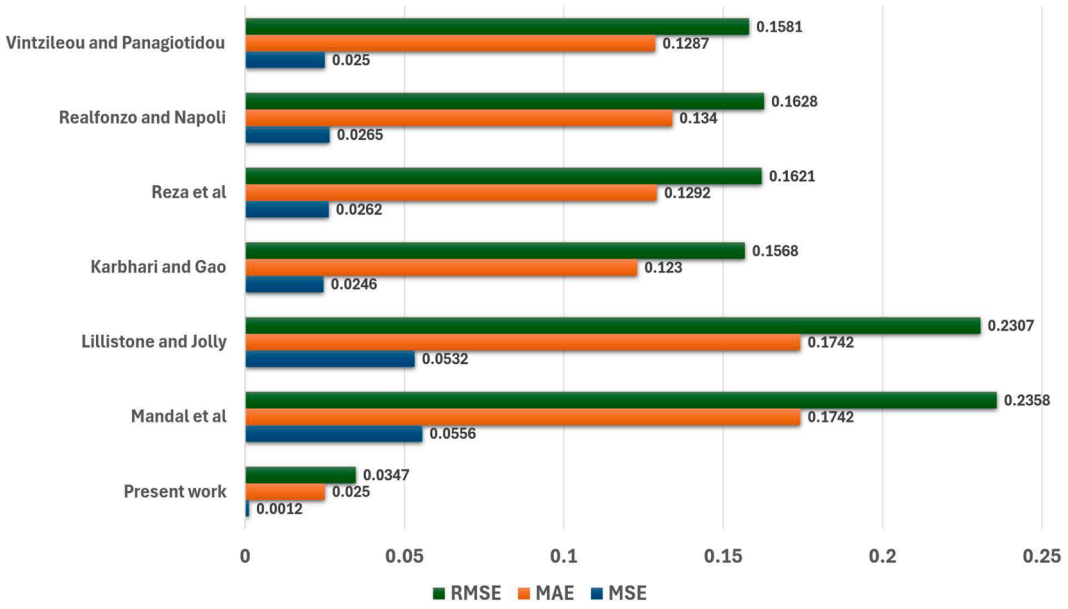

Fig. 13. Comparing RMSE, MAE, and MSE metrics for all data with all empirical models.

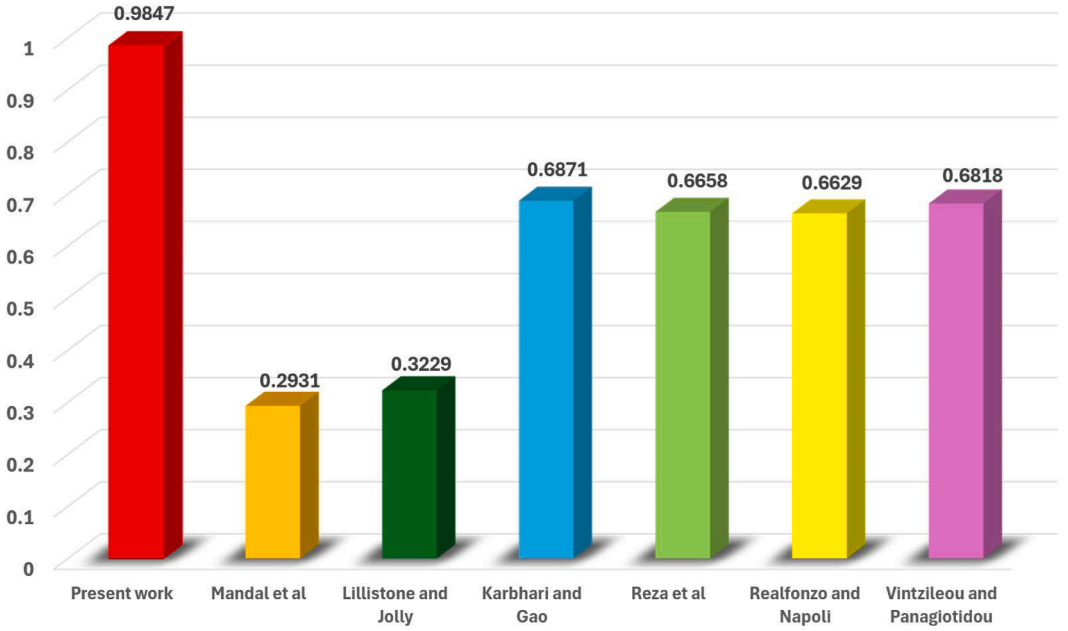

Fig. 14. Comparing R-squared metric for all data with all model.

Fig. 17 provides a comparative visualization of R-squared values for seven distinct models tested on a dataset. R-squared is a metric that quantifies the extent to which the variance in the dependent variable can be explained by the independent variable(s) in a regression model. The present work model exhibits a superior R-squared value of 0.9847, indicating an exceptional level of explained variance and predictive accuracy. Conversely, the Mandal et al. and Lillistone and Jolly models have notably lower R-squared values of 0.2931 and 0.3229, respectively, suggesting limited explanatory power and predictive capability. The Karbhari and Gao, Reza et al., Realfonzo and Napoli, and Vintzileou and Panagiotido model's register an intermediate R-squared of 0.6871, 0.6278, 0.6081, and 0.6198, respectively, and pointing to a moderately effective model. This graphical representation starkly highlights the comparative effectiveness of this work in accounting for the variability of the test dataset.

For the purpose of illustrating the comparison of mechanical diagrams across all models with experimental results, Owen's [87] experimental findings were selected, characterized by the following properties: a diameter of compression member (D) of 102 mm, height of compression member (H) of 203 mm, compressive strength of unconfined concrete (f'_{co}) of 53 MPa, tensile modulus of elasticity (E_f) of 262 GPa and ultimate tensile strength of FRP (f_f) of 4200 MPa. The diagrams were then drawn based on embedded properties, with nominal thickness of FRP reinforcement (t_f) being the only variable, altered within a range of 0 to 1.4. Moreover, a dependency between the t_f and FRP reinforcement ratio (ρ_f) was observed, resulting in changes to ρ_f as well. According to Fig. 18, it was noted that the line representing the peresent work closely approximates the experimental results. With an increase in the t_f value, an augmentation in the compressive strength of confined concrete (f'_{cc}) was observed.

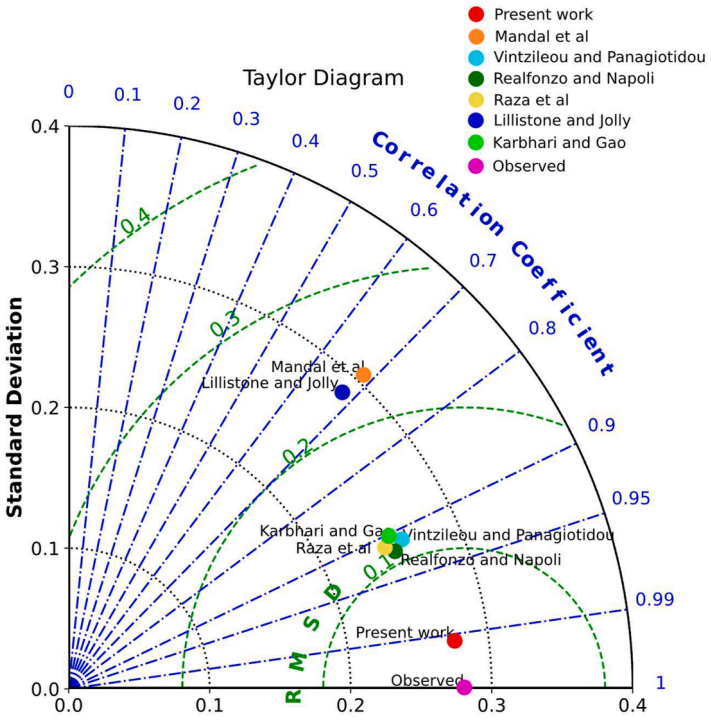

Fig. 15. Taylor diagram.

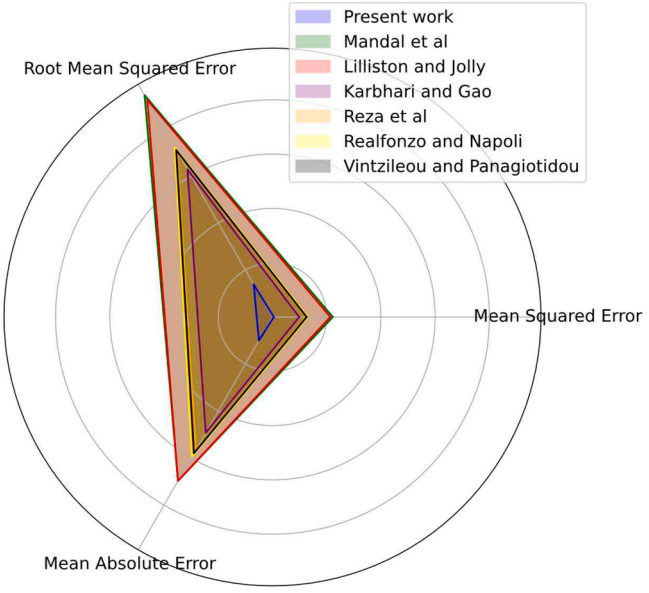

Fig. 16. RMSE, MAE and MSE results comparison for different methods for Test Dataset.

5.3. Comparison of proposed model with other ML algorithms

Table 8 presents a comparative analysis of the performance metrics for various machine learning algorithms. The table is structured to display the R-squared, MSE, MAE, and RMSE for both training and testing datasets. The methods evaluated include the proposed method, CatBoost, XgBoost, AdaBosst, GBoost, Extra Trees, and Random Forest.

The proposed method shows superior performance with the highest R^2 values of 0.9898 for the training set and 0.9572 for the test set, indicating a robust explanatory power and predictiveness. It also has the lowest MSE and RMSE on the training and testing datasets, suggesting a model with high accuracy and precision. Conversely, AdaBoost exhibits lower R^2 values, particularly on the test set with 0.7569, which might indicate overfitting or a model less capable of generalizing to new data. The Random Forest algorithm shows consistent performance across both datasets, with only a slight decrease in R^2 from training to testing. Overall, this table indicates that the proposed method may offer a robust alternative to traditional ensemble methods in the machine learning domain.

Upon evaluating the performance metrics of various machine learning algorithms, CatBoost emerged as the second-best performing method, as illustrated in Table 8. It demonstrated commendable predictive capabilities with high R-squared values of 0.9825 for the training dataset and 0.9001 for the testing dataset, alongside relatively low error metrics (MSE, MAE, and RMSE) compared to other traditional algorithms. Given its strong baseline performance, CatBoost was selected as the foundation for further refinement and development.

Building upon the robust framework of CatBoost, we introduced methodological enhancements to devise our proposed method. These enhancements aimed to address specific limitations observed in CatBoost and to further optimize the model's performance. As a result of these improvements, the proposed method not only retained the inherent strengths of CatBoost but also exhibited superior performance metrics across both training and testing datasets. The advancements led to a notable increase in R-squared values and a reduction in error rates, thereby affirming the efficacy of our modifications. The proposed method's performance with an R-squared of 0.9898 for training and 0.9572 for testing, as well as the lowest MSE, MAE, and RMSE scores, underscores its potential as a highly accurate and reliable machine learning solution.

The comparative analysis and subsequent development of the proposed method highlight the value of iterative enhancements in machine learning. By leveraging the strengths of CatBoost and incorporating targeted improvements, we have successfully developed a model that sets a new benchmark for predictive accuracy in the field.

Fig. 19 provides a detailed heatmap of the R-squared values across various parameters for the machine-learning models under consideration. The color gradient reflects the degree of variance explained by

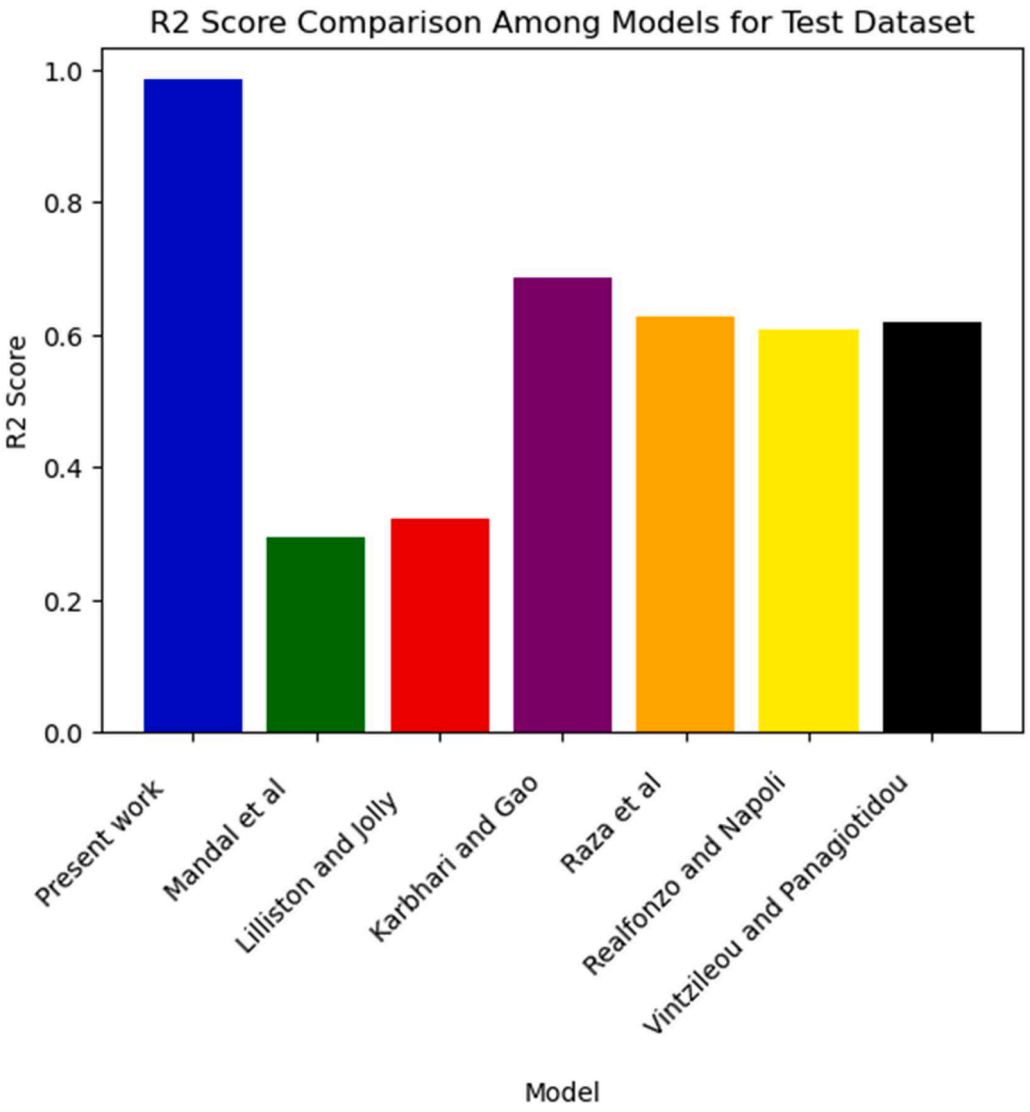

Fig. 17. R-squared results comparison for the test dataset.

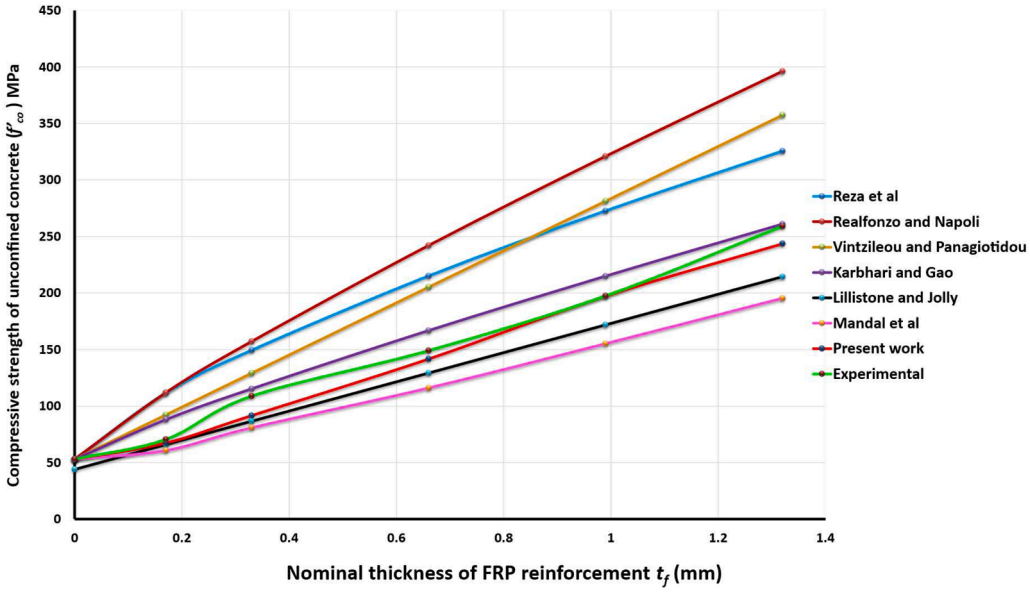

Fig. 18. Mechanical diagram comparison for all models.

Table 8
Performance metric results with other ML methods.

Methods	Data	R^2	MSE	MAE	RMSE
Proposed method	Train	**0.9898**	**0.0008**	**0.0219**	**0.0290**
	Test	**0.9572**	**0.0026**	**0.0373**	**0.0514**
CatBoost	Train	0.9825	0.0014	0.0236	0.0369
	Test	0.9001	0.0102	0.0540	0.1009
XGBoost	Train	0.9713	0.0022	0.0343	0.0474
	Test	0.8837	0.0091	0.0562	0.0955
AdaBoost	Train	0.8330	0.0131	0.0928	0.1145
	Test	0.7569	0.0191	0.1009	0.1381
GBoost	Train	0.9832	0.0009	0.0245	0.0301
	Test	0.8971	0.0065	0.0432	0.0806
Extra trees	Train	0.9822	0.0009	0.0256	0.0298
	Test	0.8775	0.0096	0.0506	0.0980
Random forest	Train	0.9848	0.0012	0.0229	0.0344
	Test	0.8778	0.0096	0.0537	0.0979

each model, with darker hues indicating higher R-squared values and, thus, greater predictive accuracy. The proposed method outperforms the others on the training set with a near-perfect score, while on the test set, it shows a slightly lower but still high score, suggesting good generalization. Other methods show varying degrees of performance, with GBoost and Random Forest also demonstrating high training scores. The test scores are consistently lower across all methods, which is typical due to the generalization gap. The color coding and the precise numeric labels on each bar provide an at-a-glance understanding of the model performances, with darker colors indicating higher scores.

In contrast, Fig. 20 illustrates a comparison chart that compares the performance of the proposed method against established machine learning algorithms across multiple metrics, including MSE, MAE, and RMSE. The error metrics for each model are split into train and test, represented by blue and orange bars, respectively. The proposed method has the lowest error rates across all three metrics on both the training and testing data, suggesting it has the best performance and generalization capability among the evaluated models. The consistency of the model's superior performance across different metrics emphasizes its robustness. In contrast, the other models exhibit higher error rates, indicating a range of effectiveness with the Random Forest model showing the highest errors in this evaluation.

5.4. Feature importance analysis of model

Machine learning models can be difficult to interpret because they are frequently seen as black boxes. In order to comprehend these models, explainable ML approaches are essential. These techniques can be used to identify the key features that determine a model's output. This study employed two approaches, namely the SHAP-based feature contribution (SHapley Additive exPlanations) [146] and Permutation Feature Importance (PFI) [147], to demonstrate the significance of each feature and its corresponding contribution to the model's predictions.

SHAP clarifies the prediction of a particular data instance by calculating each predictor's contribution to the prediction using game theory principles. Due to its theoretical strength and its fair distribution of effects, the Shapley value may be the only method capable of providing a full explanation. It addresses the lack of interpretability in certain ML algorithms by offering consistent interpretability. SHAP employs Shapley values to quantify and demonstrate the contribution of input features to the output of a model. This value is calculated by comparing the variance between the model's prediction with and without feature values. Specifically, a SHAP value is the average marginal contribution of a feature value over any potential combinations of that feature value. A positive SHAP number denotes a potential contribution (or influence) that might benefit the forecast, whereas a negative value denotes a potential contribution that could be negative [148]. The SHAP summary graphs for the proposed model are displayed in Fig. 21. These charts demonstrate the effects of characteristics with greater and lower values on the SHAP values. Additionally, the attributes are arranged on the Y axis in descending order of importance. As can be seen in Fig. 21, higher values of compressive strength of unconfined concrete and ultimate tensile strength of FRP have a positive impact on the prediction, while lower values of FRP reinforcement ratio and thickness of FRP have a negative impact. Other features make a very tiny contribution.

The mean SHAP value offers a comprehensive assessment of the significance of a feature across all instances within a given dataset, as

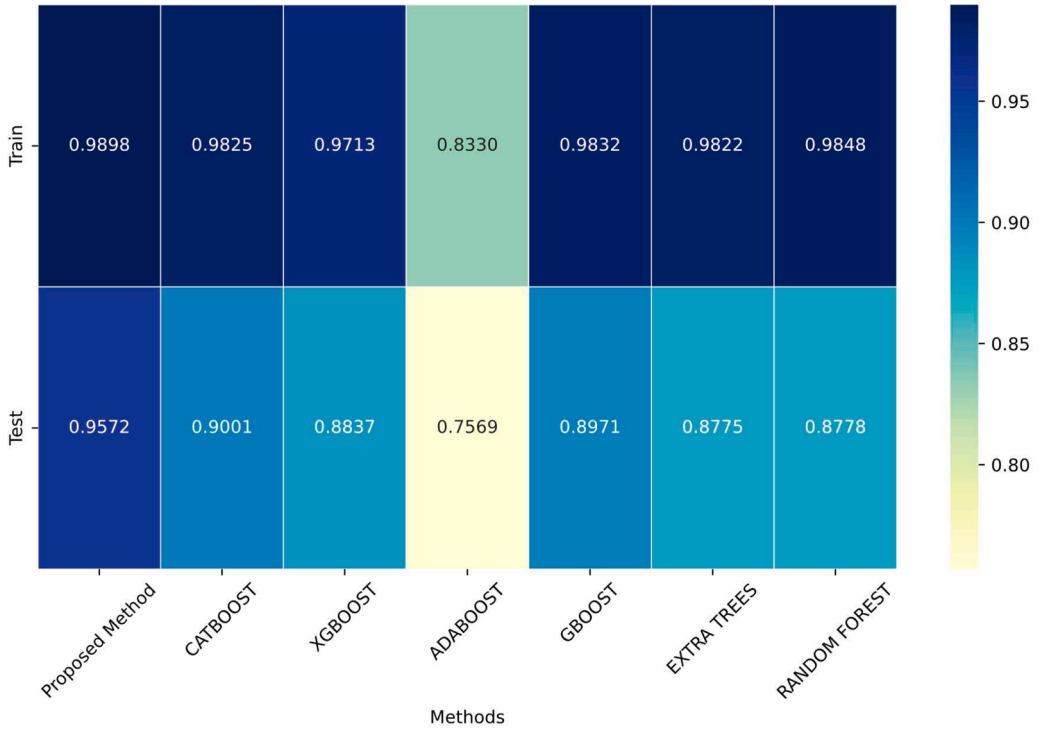

Fig. 19. R-squared results comparison for different ML methods for test and train dataset.

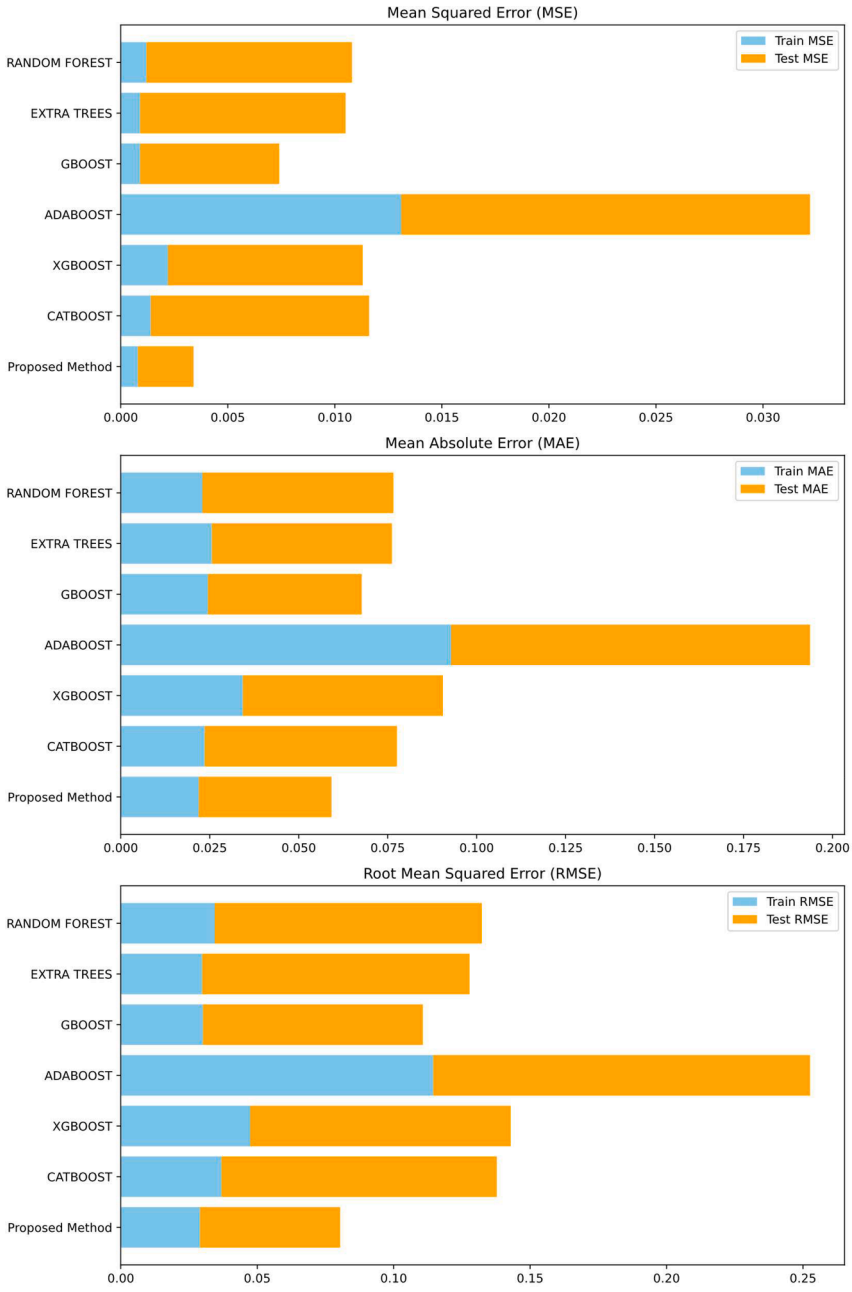

Fig. 20. RMSE, MAE and MSE results for all ML methods for test and train dataset.

shown in Fig. 22. The calculation involves determining the average of the absolute SHAP values for a specific feature across all instances. A feature with a high mean SHAP value indicates that it substantially influences the model's prediction, regardless of whether this influence is positive or negative. In contrast, a feature with a low mean SHAP value suggests that its contribution to the model's prediction is generally very small.

The aforementioned metric can be employed to assess and contrast the relative significance of various attributes within a machine-learning model. Nevertheless, it is crucial to remember that although mean SHAP values provide a broad understanding of the significance of features, they do not reveal the specific impact of each feature on individual predictions, which is the primary purpose of SHAP values. In addition, the scatter plot of each feature for SHAP value is shown in Fig. 23.

In contrast to methods like SHAP, which highlight which characteristics were more significant in creating a particular prediction, the PFI method displays the features that influence the model's overall performance. The concept underlying PFI is straightforward. The input variables that contribute to prediction possess substantial informational value. The quality of predictions will decrease when the information is disrupted by randomly shuffling feature values. If the drop in quality is small, then the original predictor's information was not crucial to making predictions, and the model still does reasonably well even without it. Conversely, a considerable reduction in value suggests that the initial predictor had a notable impact on the accuracy of predictions [148]. This analysis provides a critical understanding of the decision-making process of the model. Fig. 24 reveals that the CFRP reinforcement ratio and compressive strength of unconfined concrete are the most influential factors in predicting the compressive strength of confined concrete in the proposed model. Lastly, it seems that the other features do not significantly impact the predictions.

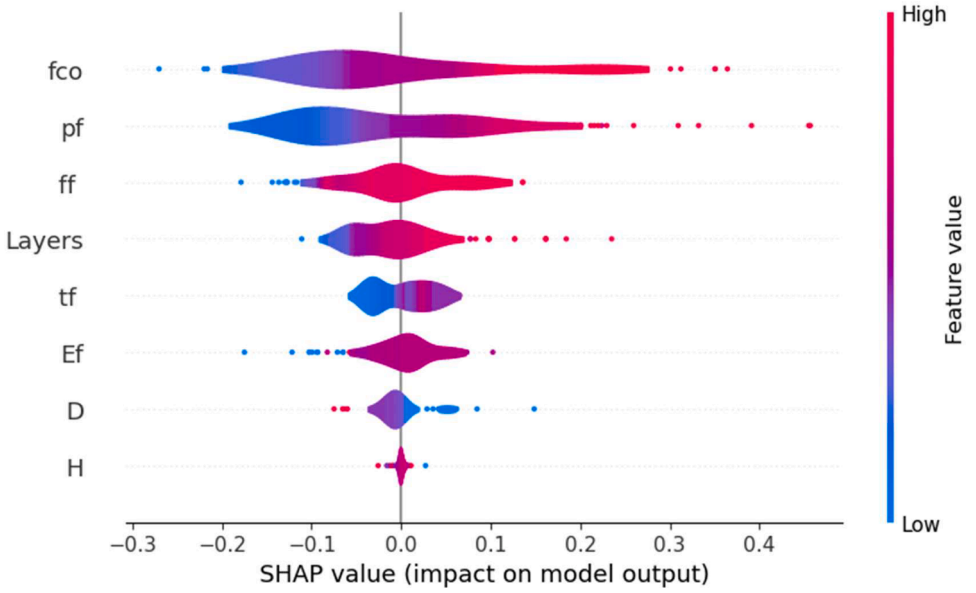

Fig. 21. The SHAP diagram for impact of features.

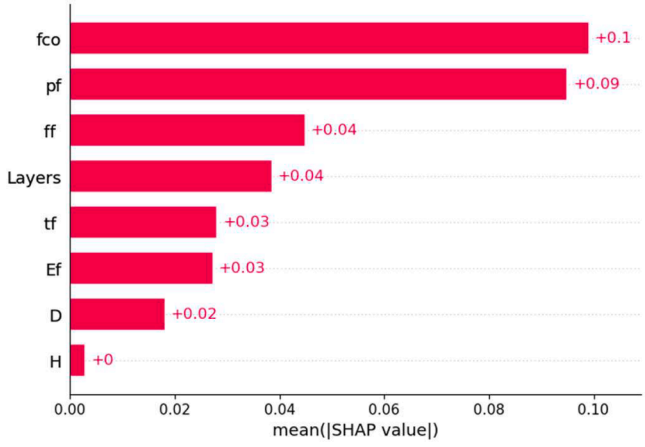

Fig. 22. Effects of all features for compressive strength of CFRP concrete.

5.5. Graphical user interface (GUI) of model

The intricately engineered Graphical User Interface (GUI) is developed specifically for modeling the compressive strength of CFRP-CC. This interface, characterized by its user-friendly design, facilitates direct engagement with the research findings, thereby easing the computation of compressive strength values for CFRP-CC. The design of this GUI, which transcends mere scientific accuracy, guarantees the pragmatic application of research outcomes in real-world contexts. Serving as an intermediary between the research's inherent complexities and its practical execution, the GUI renders the research's critical insights more comprehensible and applicable to an extensive audience. The open-source platform, as demonstrated in Fig. 25, exhibits a design that is easily navigable for users (The GUI file is publicly available at https://nimakhodadadi.com/software).

6. Conclusion and future work

The main goal of the study was to create advanced models by utilizing the latest machine learning techniques for improving predictions on the strength of Carbon Fiber Reinforced Polymer-Confined Concrete (CFRP-CC) samples. A large dataset containing 916 samples was utilized for model development, which combines Particle Swarm Optimization (PSO) with Categorical Boosting algorithms (PSO-CatBoost). Following the model's development, the study compared it against six other models based on real experimental data. Additionally, a novel and thorough comparative analysis was conducted to evaluate the PSO-CatBoost model against six state-of-the-art machine-learning models, including CatBoost, XgBoost, AdaBoost, GBoost, Extra Trees, and Random Forest. The SHAP (Shapley Additive exPlanations) method was employed to understand the significance of various predictors and their

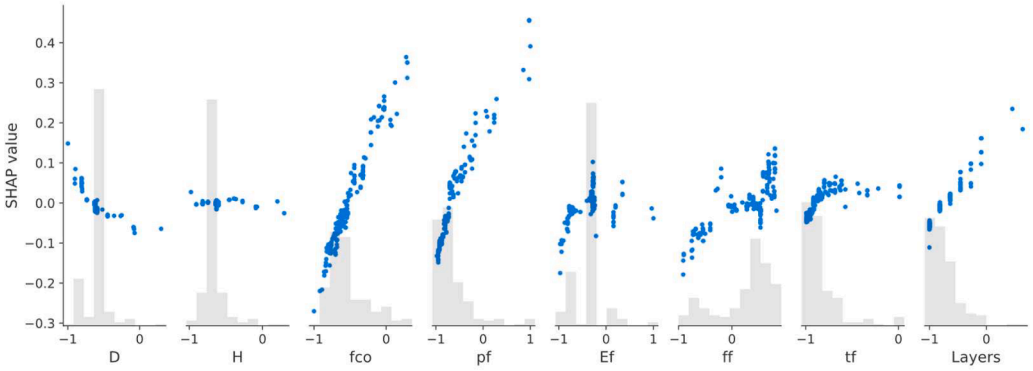

Fig. 23. Scatter plot of each feature for SHAP value.

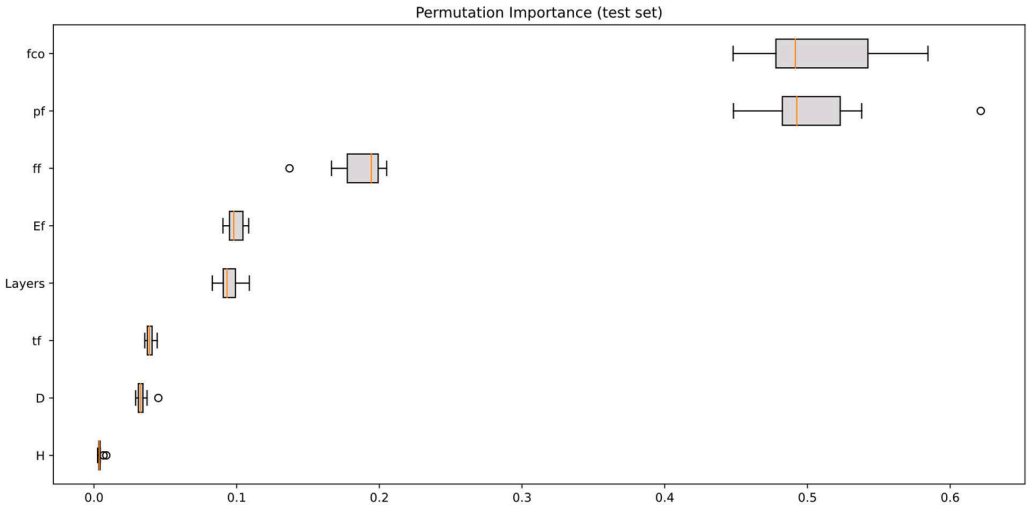

Fig. 24. The box plot of permutation importance for features of the dataset.

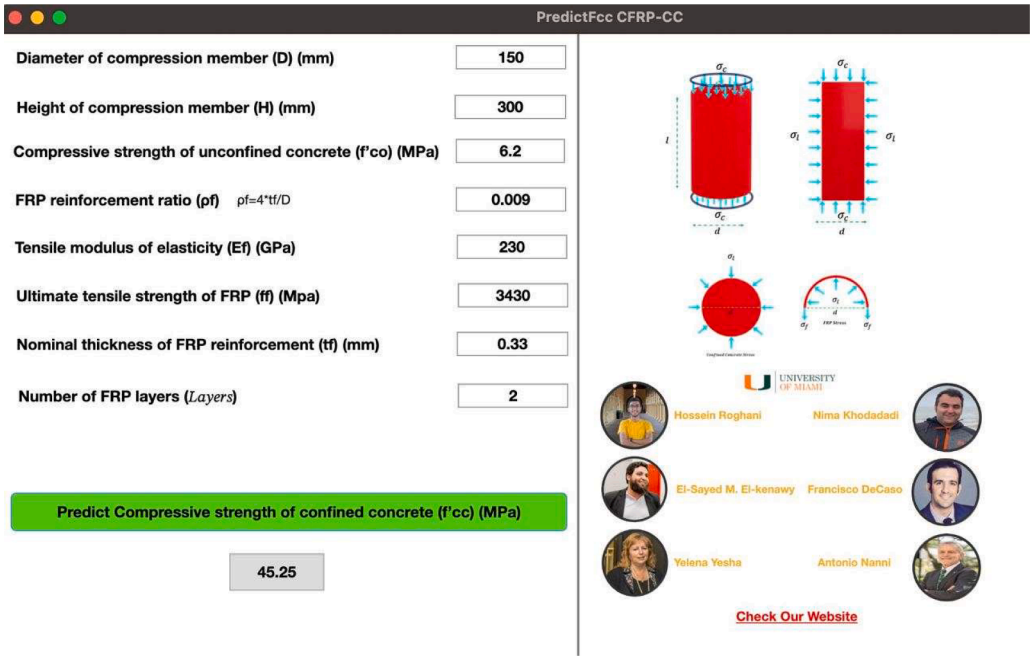

Fig. 25. GUI-based application developed to predict compressive strength values for CFRP-CC.

interactions. Feature importance evaluations revealed that the compressive strength of unconfined concrete (f'_{co}) along with the FRP reinforcement ratio (ρ_f) emerged as the paramount predictors for the compressive strength of CFRP-CC specimens. An analysis of the dataset disclosed that the strength of unconfined concrete is pivotal in appraising the efficacy of confinement, and a salient association was detected between the axial rigidity ($\rho_f E_f$) of the composite jacket and the compressive strength under confinement.

The results demonstrated that the incorporation of PSO to enhance these algorithms significantly improved the precision of the predictive models compared to their basic versions. The comprehensive analysis strongly supports the superiority of machine learning methods over traditional approaches for complex structural predictions and design problem solutions. The performance of these algorithms, however, is dependent on their robustness and the depth and detail of the dataset. The implementation of boosting algorithms was highlighted for their ability to improve predictive accuracy due to their proficiency in handling diverse data and ensuring precise model representation. Among the evaluated models, the PSO-CatBoost model was distinguished by achieving a high coefficient of determination, marked at 0.9847, and was notably effective in reducing both mean squared error and root mean squared error when compared with experimental benchmarks.

It is recommended for future research to focus on applying these methodologies to enhance predictive accuracy across additional experimental models. Moreover, the exploration of alternative optimization algorithms in place of PSO is suggested to achieve more accurate results. The application of this model is expected to extend to other areas within the concrete and civil engineering disciplines.

CRediT authorship contribution statement

Nima Khodadadi: Writing – original draft, Visualization, Software, Methodology, Formal analysis, Conceptualization. **Hossein Roghani:** Writing – original draft, Data curation. **Francisco De Caso:** Writing – review & editing, Resources, Investigation. **El-Sayed M. El-kenawy:**

Writing – review & editing, Visualization, Validation. **Yelena Yesha:** Investigation, Formal analysis. **Antonio Nanni:** Writing – review & editing, Supervision, Project administration.

Declaration of competing interest

The authors declare that they have no known competing financial interests or personal relationships that could have appeared to influence the work reported in this paper.

Data availability

Data will be made available on request.

Acknowledgments

The authors gratefully acknowledge the financial support from the National Science Foundation I/U-CRC Center for Integration of Composites into Infrastructure (CICI) under grant #1916342. The authors express their sincere gratitude to the Inter-American Cement Federation (FICEM) for their invaluable support and assistance during the internship period.

Supplementary materials

Supplementary material associated with this article can be found, in the online version, at doi:10.1016/j.tws.2024.111763.

References

[1] T. Ozbakkaloglu, J.C. Lim, T. Vincent, FRP-confined concrete in circular sections: review and assessment of stress–strain models, Eng. Struct. 49 (2013) 1068–1088.
[2] J. Jiang, P. Xiao, B. Li, A novel triaxial test system for concrete under passive confinement, J. Test. Eval. 46 (2017) 0160547.
[3] Y. Wang, H. Wu, Size effect of concrete short columns confined with aramid FRP jackets, J. Compos. Constr. 15 (2011) 535–544.
[4] P. Faustino, C. Chastre, Analysis of load–strain models for RC square columns confined with CFRP, Compos. B Eng. 74 (2015) 23–41.
[5] L. Lam, J.G. Teng, Design-oriented stress–strain model for FRP-confined concrete, Constr. Build. Mater. 17 (2003) 471–489.
[6] M. Samaan, A. Mirmiran, M. Shahawy, Model of concrete confined by fiber composites, J. Struct. Eng. 124 (1998) 1025–1031.
[7] A. Mirmiran, M. Shahawy, Novel FRP-concrete composite construction for the infrastructure, (1995).
[8] C.-C. Hou, L.-H. Han, Q.-L. Wang, C. Hou, Flexural behavior of circular concrete filled steel tubes (CFST) under sustained load and chloride corrosion, Thin-Walled Struct. 107 (2016) 182–196.
[9] Y. Ouyang, A.K.H. Kwan, Finite element analysis of square concrete-filled steel tube (CFST) columns under axial compressive load, Eng. Struct. 156 (2018) 443–459.
[10] A. Mirmiran, M. Shahawy, Behavior of concrete columns confined by fiber composites, J. Struct. Eng. 123 (1997) 583–590.
[11] S.M.P. Rashid, A. Bahrami, Structural performance of infilled steel–concrete composite thin-walled columns combined with FRP and CFRP: a comprehensive review, Materials (Basel) 16 (2023) 1564.
[12] C.G. Papakonstantinou, Fiber reinforced polymer (FRP) confined circular columns: compressive strength assessment, J. Eng. Sci. Technol. Rev. 13 (2020).
[13] J. Zhou, F. Bi, Z. Wang, J. Zhang, Experimental investigation of size effect on mechanical properties of carbon fiber reinforced polymer (CFRP) confined concrete circular specimens, Constr. Build. Mater. 127 (2016) 643–652.
[14] S. Pessiki, K.A. Harries, J.T. Kestner, R. Sause, J.M. Ricles, Axial behavior of reinforced concrete columns confined with FRP jackets, J. Compos. Constr. 5 (2001) 237–245.
[15] T. Jiang, J.G. Teng, Analysis-oriented stress–strain models for FRP–confined concrete, Eng. Struct. 29 (2007) 2968–2986.
[16] H. Toutanji, Stress-strain characteristics of concrete columns externally confined with advanced fiber composite sheets, Mater. J. 96 (1999) 397–404.
[17] M. Shahawy, A. Mirmiran, T. Beitelman, Tests and modeling of carbon-wrapped concrete columns, Compos. B Eng. 31 (2000) 471–480.
[18] Z. Huang, Z. Chen, Comparison of different machine learning algorithms for predicting the SAGD production performance, J. Pet. Sci. Eng. 202 (2021) 108559.
[19] S.-Y. Zhang, S.-Z. Chen, X. Jiang, W.-S. Han, Data-driven Prediction of FRP Strengthened Reinforced Concrete Beam Capacity Based On Interpretable Ensemble Learning algorithms, in: Structures, Elsevier, 2022, pp. 860–877.
[20] S.-Z. Chen, D.-C. Feng, W.-J. Wang, E. Taciroglu, Probabilistic machine-learning methods for performance prediction of structure and infrastructures through natural gradient boosting, J. Struct. Eng. 148 (2022) 4022096.
[21] M. Berradia, E.H. Meziane, A. Raza, M. Ahmed, Q. uz Z. Khan, F. Shabbir, Prediction of ultimate strain and strength of CFRP-wrapped normal and high-strength concrete compressive members using ANN approach, Mech. Adv. Mater. Struct. (2023) 1–23.
[22] A. Kaveh, N. Khavaninzadeh, Efficient Training of Two ANNs Using Four Meta-Heuristic Algorithms For Predicting the FRP strength, in: Structures, Elsevier, 2023, pp. 256–272.
[23] H. Li, D. Yang, T. Hu, Data-driven model for predicting the compressive strengths of GFRP-confined reinforced concrete columns, Buildings 13 (2023) 1309.
[24] I. Ilyas, A. Zafar, M.F. Javed, F. Farooq, F. Aslam, M.A. Musarat, N.I. Vatin, Forecasting strength of CFRP confined concrete using multi expression programming, Materials (Basel) 14 (2021) 7134.
[25] B. Keshtegar, A. Gholampour, D.-K. Thai, O. Taylan, N.-T. Trung, Hybrid regression and machine learning model for predicting ultimate condition of FRP-confined concrete, Compos. Struct. 262 (2021) 113644.
[26] W. Chen, J. Xu, M. Dong, Y. Yu, M. Elchalakani, F. Zhang, Data-driven analysis on ultimate axial strain of FRP-confined concrete cylinders based on explicit and implicit algorithms, Compos. Struct. 268 (2021) 113904.
[27] R. Elshawi, M. Maher, S. Sakr, Automated machine learning: state-of-the-art and open challenges, ArXiv Preprint ArXiv:1906.02287 (2019).
[28] M. Feurer, F. Hutter, Hyperparameter optimization, Automated Machine Learning: Methods, Systems, Challenges, 2019, pp. 3–33.
[29] A. Kaveh, S. Talatahari, N. Khodadadi, Stochastic paint optimizer: theory and application in civil engineering, Eng. Comput. 38 (2022) 1921–1952, https://doi.org/10.1007/s00366-020-01179-5.
[30] J. Kennedy, R. Eberhart, Particle swarm optimization, in: Proceedings of ICNN'95-International Conference on Neural Networks, IEEE, 1995, pp. 1942–1948.
[31] S. Mandal, A. Hoskin, A. Fam, Influence of concrete strength on confinement effectiveness of fiber-reinforced polymer circular jackets, ACI. Struct. J. 102 (2005) 383.
[32] V.M. Karbhari, Y. Gao, Composite jacketed concrete under uniaxial compression—verification of simple design equations, J. Mater. Civil Eng. 9 (1997) 185–193.
[33] D. Lillistone, C.K. Jolly, An innovative form of reinforcement for concrete columns using advanced composites, Struct. Eng. 78 (2000).
[34] A. Raza, Q. uz Z. Khan, A. Ahmad, Prediction of axial compressive strength for FRP-confined concrete compression members, KSCE J. Civil Eng. 24 (2020) 2099–2109.
[35] R. Realfonzo, A. Napoli, Concrete confined by FRP systems: confinement efficiency and design strength models, Compos. B Eng. 42 (2011) 736–755.
[36] E. Vintzileou, E. Panagiotidou, An empirical model for predicting the mechanical properties of FRP-confined concrete, Constr. Build. Mater. 22 (2008) 841–854.
[37] M.K. Valasaki, C.G. Papakonstantinou, Fiber reinforced polymer (FRP) confined circular concrete columns: an experimental overview, Buildings 13 (2023), https://doi.org/10.3390/buildings13051248.
[38] Building code requirements for structural concrete (ACI 318-19) commentary on building code requirements for structural concrete (ACI 318R-19) IN-LB, 2019.
[39] ACI Committee 440, Guide for the Design and Construction of Externally Bonded FRP Systems for Strengthening Concrete Structures (ACI 440.2R-17), American Concrete Institute, Farmington Hills, MI., 2017.
[40] B. Erdil, U. Akyuz, I.O. Yaman, Mechanical behavior of CFRP confined low strength concretes subjected to simultaneous heating–cooling cycles and sustained loading, Mater. Struct. 45 (2012) 223–233.
[41] A. Ilki, N. Kumbasar, V. Koc, Low strength concrete members externally confined with FRP sheets, Struct. Eng. Mech. Int. J. 18 (2004) 167–194.
[42] M. Karantzikis, C.G. Papanicolaou, C.P. Antonopoulos, T.C. Triantafillou, Experimental investigation of nonconventional confinement for concrete using FRP, J. Compos. Constr. 9 (2005) 480–487.
[43] T.H. Pon, Y.F. Li, B.J. Shih, M.S. Han, G.D. Chu, Y.J. Chiu, J.C. Lin, Y.S. Cheng, Experiments of scale effects on the strength of FRP reinforced concrete, in: Proceedings of the 4th National Conference on Structural Engineering, Taipei, Taiwan, 1998, pp. 2133–2140.
[44] K. Abdelrahman, R. El-Hacha, Behavior of large-scale concrete columns wrapped with CFRP and SFRP sheets, J. Compos. Constr. 16 (2012) 430–439.
[45] C. Aire, R. Gettu, J.R. Casas, S. Marques, D. Marques, Concrete laterally confined with fibre-reinforced polymers (FRP): experimental study and theoretical model, Materiales de Construcción 60 (2010) 19–31.
[46] R.-K. Akogbe, M. Liang, Z.-M. Wu, Size effect of axial compressive strength of CFRP confined concrete cylinders, Int. J. Concr. Struct. Mater. 5 (2011) 49–55.
[47] Y. Al-Salloum, N. Siddiqui, Compressive strength prediction model for FRP-confined concrete, in: Proceedings, Ninth International Symposium on Fiber Reinforced Polymer Reinforcement for Concrete Structures, 2009, pp. 97–106.
[48] R. Benzaid, H. Mesbah, N.E. Chikh, FRP-confined concrete cylinders: axial compression experiments and strength model, J. Reinf. Plast. Compos. 29 (2010) 2469–2488.
[49] J.F. Berthet, E. Ferrier, P. Hamelin, Compressive behavior of concrete externally confined by composite jackets. Part A: experimental study, Constr. Build. Mater. 19 (2005) 223–232.
[50] L. Bisby, W.A. Take, A. Caspary, Quantifying strain variation in FRP confined concrete using digital image correlation: proof-of-concept and initial results, in: Proc., 1st Asia-Pacific Conf. on FRP in Structures, Dept. of Civil Engineering, Hong Kong, Univ. of Hong Kong, 2007, pp. 599–604.

[51] L.A. Bisby, J.-F. Chen, S.Q. Li, T.J. Stratford, N. Cueva, K. Crossling, Strengthening fire-damaged concrete by confinement with fibre-reinforced polymer wraps, Eng. Struct. 33 (2011) 3381–3391.
[52] H. Bouchelaghem, A. Bezazi, F. Scarpa, Compressive behaviour of concrete cylindrical FRP-confined columns subjected to a new sequential loading technique, Compos. B Eng. 42 (2011) 1987–1993.
[53] G. Campione, N. Miraglia, N. Scibilia, Comprehensive behaviour Of RC members strengthened with carbon fiber reinforced plastic layers, WIT Trans. Built Environ. 57 (2001).
[54] S.A. Carey, K.A. Harries, Axial behavior and modeling of confined small-, medium-, and large-scale circular sections with carbon fiber-reinforced polymer jackets, ACI. Struct. J. 102 (2005) 596.
[55] C. Chastre, M.A.G. Silva, Monotonic axial behavior and modelling of RC circular columns confined with CFRP, Eng. Struct. 32 (2010) 2268–2277.
[56] C. Cui, S.A. Sheikh, Experimental study of normal-and high-strength concrete confined with fiber-reinforced polymers, J. Compos. Constr. 14 (2010) 553–561.
[57] L. De Lorenzis, F. Micelli, A.La Tegola, Influence of specimen size and resin type on the behaviour of FRP-confined concrete cylinders, Adv. Polym. Compos. Struct. Appl. Constr. (2002) 231–239.
[58] M. Demers, K.W. Neale, Strengthening of concrete columns with unidirectional composite sheets, Develop. Short Medium Span Bridge Eng. (1994) 895–905.
[59] V.D. da Silva, J.M.C. Santos, Strengthening of axially loaded concrete cylinders by surface composites, Compos. Constr. (2001) 257–262.
[60] H.M. Elsanadedy, Y.A. Al-Salloum, S.H. Alsayed, R.A. Iqbal, Experimental and numerical investigation of size effects in FRP-wrapped concrete columns, Constr. Build. Mater. 29 (2012) 56–72.
[61] J. Evans, M. Kocman, T. Kretschmer, Hybrid FRP Confined Concrete columns, Honours, The School of Civil, Environmental and Mining Engineering, Univ. of Adelaide., Adelaide, Australia, 2008.
[62] M.F. Green, L.A. Bisby, A.Z. Fam, V.K.R. Kodur, FRP confined concrete columns: behaviour under extreme conditions, Cem. Concr. Compos. 28 (2006) 928–937.
[63] T.G. Harmon, K.T. Slattery, Advanced composite confinement of concrete. Advanced Composite Materials in Bridges and Structures, 1992, pp. 299–306.
[64] K.A. Harries, G. Kharel, Behavior and modeling of concrete subject to variable confining pressure, Mater. J. 99 (2002) 180–189.
[65] M. Hosotani, K. Kawashima, J. Hoshikuma, A model for confinement effect for concrete cylinders confined by carbon fiber sheets, 1997.
[66] I. Howie, V.M. Karbhari, Effect of materials architecture on strengthening efficiency of composite wraps for deteriorating columns in the North-East. Infrastructure: New Materials and Methods of Repair, ASCE, 1994, pp. 199–206.
[67] A. Ilki, N. Kumbasar, V. Koc, Strength and deformability of low strength concrete confined by carbon fiber composite sheets, in: Proc. ASCE 15th Engineering Mechanics Conference, Columbia University New York, 2002.
[68] M.S.I. Choudhury, A. Amin, M.M. Islam, A. Hasnat, Effect of confining pressure distribution on the dilation behavior in FRP-confined plain concrete columns using stone, brick and recycled aggregates, Constr. Build. Mater. 102 (2016) 541–551.
[69] C.A. Issa, The effect of elevated temperatures on CFRP wrapped concrete cylinders, in: Proceedings of the 8th International Symposium on Fiber-Reinforced Polymer Reinforcement for Concrete Structures, by TC Triantafillou, Patras, Greece, 2007.
[70] C.A. Issa, P. Chami, G. Saad, Compressive strength of concrete cylinders with variable widths CFRP wraps: experimental study and numerical modeling, Constr. Build. Mater. 23 (2009) 2306–2318.
[71] C. Jiang, Y.-F. Wu, J.-F. Jiang, Effect of aggregate size on stress-strain behavior of concrete confined by fiber composites, Compos. Struct. 168 (2017) 851–862.
[72] G. Karam, M. Tabbara, Corner effects in CFRP-wrapped square columns, Magaz. Concr. Res. 56 (2004) 461–464.
[73] S. Kono, M. Inazumi, T. Kaku, Evaluation of confining effects of CFRP sheets on reinforced concrete members, in: Second International Conference on Composites in InfrastructureNational Science Foundation, 1998.
[74] L. Lam, J.G. Teng, Ultimate condition of fiber reinforced polymer-confined concrete, J. Compos. Constr. 8 (2004) 539–548.
[75] L. Lam, J.G. Teng, C.H. Cheung, Y. Xiao, FRP-confined concrete under axial cyclic compression, Cem. Concr. Compos. 28 (2006) 949–958.
[76] J.-Y. Lee, C.-K. Yi, H.-S. Jeong, S.-W. Kim, J.-K. Kim, Compressive response of concrete confined with steel spirals and FRP composites, J. Compos. Mater. 44 (2010) 481–504.
[77] Y. Li, T. Fang, C. Chern, A constitutive model for concrete cylinder confined by steel reinforcement and carbon fibre sheet, in: Proc., Pacific Conf. on Earthquake Engineering, Univ. of Canterbury Christchurch, New Zealand, 2003.
[78] P. Li, Y.-F. Wu, R. Gravina, Cyclic response of FRP-confined concrete with post-peak strain softening behavior, Constr. Build. Mater. 123 (2016) 814–828.
[79] C.-T. Lin, Y.-F. Li, An effective peak stress formula for concrete confined with carbon fiber reinforced plastics, Canad. J. Civil Eng. 30 (2003) 882–889.
[80] S. Matthys, L. Taerwe, K. Audenaert, Tests on axially loaded concrete columns confined by fiber reinforced polymer sheet wrapping, Spec. Public. 188 (1999) 217–228.
[81] F. Micelli, J.J. Myers, S. Murthy, Effect of environmental cycles on concrete cylinders confined with FRP, in: Proceedings of CCC2001 International Conference on Composites in Construction, Porto, Portugal, 2001.
[82] K. MIYAUCHI, Estimation of strengthening effects with Crbon Feber sheet for concrete column, in: Proceedings of the 3rd International Symposium on Non-Metallic (FRP) Reinforcement for Concrete Structures, Japan Concrete Institute, 1997, pp. 217–224.
[83] K. Miyauchi, S. Inoue, T. Kuroda, A. Kobayashi, Strengthening effects with carbon fiber sheet for concrete column, Proc. Jpn. Concr. Inst. 21 (1999) 1453–1458.
[84] R. Modarelli, F. Micelli, O. Manni, FRP-confinement of hollow concrete cylinders and prisms, in: Proceedings of the 7th International Symposium on Fiber Reinforced Polymer Reinforcement of Reinforced Concrete Structures, Citeseer, 2005, pp. 1029–1046.
[85] M.L. Moretti, E. Arvanitopoulos, Overlap length for confinement of carbon and glass FRP-jacketed concrete columns, Compos. Struct. 195 (2018) 14–25.
[86] J.M.C. Ongpeng, Retrofitting RC circular columns using CFRP sheets as confinement, in: Symposium on Infrastructure Development and the Environment, 2006, pp. 1–10.
[87] L.M. Owen, Stress-Strain Behavior of Concrete Confined By Carbon Fiber Jacketing, University of Washington, 1998.
[88] F. Picher, Confinement of concrete cylinders with CFRP, Fiber Composites in Infrastructure, in: Proceedings of the First International Conference on Composites in Infrastructure, 1996, pp. 829–841.
[89] J. Piekarczyk, W. Piekarczyk, S. Blazewicz, Compression strength of concrete cylinders reinforced with carbon fiber laminate, Constr. Build. Mater. 25 (2011) 2365–2369.
[90] B.K. Purba, A.A. Mufti, Investigation of the behavior of circular concrete columns reinforced with carbon fiber reinforced polymer (CFRP) jackets, Canad. J. Civil Eng. 26 (1999) 590–596.
[91] P. Rochette, P. Labossiere, Axial testing of rectangular column models confined with composites, J. Compos. Constr. 4 (2000) 129–136.
[92] T. Rousakis, C.-S. You, L. de Lorenzis, V. Tamužs, R. Tepfers, Concrete Cylinders Confined By CFRP Sheets Subjected to Cyclic Axial Compressive load, in: Fibre-Reinforced Polymer Reinforcement for Concrete Structures: (In 2 Volumes), World Scientific, 2003, pp. 571–580.
[93] N. Saenz, C.P. Pantelides, Short and medium term durability evaluation of FRP-confined circular concrete, J. Compos. Constr. 10 (2006) 244–253.
[94] D. Santarosa, A. Campos Filho, A.J. Beber, J.L. Campagnolo, Concrete columns confined with CFRP sheets, in: Proceedings of the International Conference on FRP Composites in Civil Engineering, The Netherlands, Elsevier Science Amsterdam, 2001, pp. 301–308.
[95] I. Shehata, L.A.V Carneiro, L.C.D. Shehata, Strength of confined short concrete columns, in: Proc., 8th Int. Symp. on Fiber Reinforced Polymer Reinforcement for Concrete Structures, 2007, pp. 1–10.
[96] S.T. Smith, S.J. Kim, H. Zhang, Behavior and effectiveness of FRP wrap in the confinement of large concrete cylinders, J. Compos. Constr. 14 (2010) 573–582.
[97] X. Song, X. Gu, Y. Li, T. Chen, W. Zhang, Mechanical behavior of FRP-strengthened concrete columns subjected to concentric and eccentric compression loading, J. Compos. Constr. 17 (2013) 336–346.
[98] J.F. Stanton, L.M. Owen, The influence of concrete strength and confinement type on the response of FRP-confined concrete cylinders, Spec. Public. 238 (2006) 347–362.
[99] R. Suter, R. Pinzelli, Confinement of concrete columns with FRP sheets, in: Proc., 5th Int. Conf. on Fibre Reinforced Plastics for Reinforced Concrete Structures, 2001, pp. 793–802.
[100] V. Tamuzs, V. Valdmanis, R. Tepfers, K. Gylltoft, Stability analysis of CFRP-wrapped concrete columns strengthened with external longitudinal CFRP sheets, Mech. Compos. Mater. 44 (2008) 199–208.
[101] M. Thériault, K.W. Neale, S. Claude, Fiber-reinforced polymer-confined circular concrete columns: investigation of size and slenderness effects, J. Compos. Constr. 8 (2004) 323–331.
[102] M. Touhari, R. Mitiche-Kettab, Behaviour of FRP confined concrete cylinders: experimental investigation and strength model, Periodica Polytechnica Civil Eng. 60 (2016) 647–660.
[103] H. Toutanji, Y. Deng, Performance of concrete columns strengthened with fiber reinforced polymer composite sheets, Adv. Compos. Mater. 10 (2001) 159–168.
[104] V. Valdmanis, L. De Lorenzis, T. Rousakis, R. Tepfers, Behaviour and capacity of CFRP-confined concrete cylinders subjected to monotonic and cyclic axial compressive load, Struct. Concr. 8 (2007) 187–200.
[105] T. Vincent, T. Ozbakkaloglu, Influence of concrete strength and confinement method on axial compressive behavior of FRP confined high-and ultra high-strength concrete, Compos. B Eng. 50 (2013) 413–428.
[106] P. Wang, K.-K. Cheong, RC columns strengthened by FRP under uniaxial compression, in: Proc., Int. Conf. on FRP Composites in Civil Engineering, 2001, pp. 327–334.
[107] L.-M. Wang, Y.-F. Wu, Effect of corner radius on the performance of CFRP-confined square concrete columns: test, Eng. Struct. 30 (2008) 493–505.
[108] Z. Wang, D. Wang, S.T. Smith, D. Lu, Experimental testing and analytical modeling of CFRP-confined large circular RC columns subjected to cyclic axial compression, Eng. Struct. 40 (2012) 64–74.
[109] K. Watanabe, H. Nakamura, Y. Honda, M. Toyoshima, M. Iso, T. Fujimaki, M. Kaneto, N. Shirai, Confinement effect of FRP sheet on strength and ductility of concrete cylinders under uniaxial compression, in: non-Metallic (FRP) Reinforcement for Concrete Structures, in: Proceedings of the Third International Symposium, Japan Concrete Institute, 1997, pp. 233–240.
[110] Y.-F. Wu, C. Jiang, Effect of load eccentricity on the stress–strain relationship of FRP-confined concrete columns, Compos. Struct. 98 (2013) 228–241.
[111] G. Wu, Z.S. Wu, Z.T. Lu, Y.B. Ando, Structural performance of concrete confined with hybrid FRP composites, J. Reinf. Plast. Compos. 27 (2008) 1323–1348.
[112] Y. Xiao, H. Wu, Compressive behavior of concrete confined by carbon fiber composite jackets, J. Mater. Civil Eng. 12 (2000) 139–146.

[113] Z. Yan, C.P. Pantelides, L.D. Reaveley, Fiber-reinforced polymer jacketed and shape-modified compression members: i-experimental behavior, ACI. Struct. J. 103 (2006) 885.
[114] M.N. Youseff, Stress-Strain Model for Concrete Confined By FRP Composites, University of California, Irvine, 2007.
[115] M.N. Youssef, M.Q. Feng, A.S. Mosallam, Stress–strain model for concrete confined by FRP composites, Compos. B Eng. 38 (2007) 614–628.
[116] S. Zhang, L. Ye, Y.-W. Mai, A study on polymer composite strengthening systems for concrete columns, Appl. Compos. Mater. (Dordr) 7 (2000) 125–138.
[117] W. Wang, M.N. Sheikh, A.Q. Al-Baali, M.N.S. Hadi, Compressive behaviour of partially FRP confined concrete: experimental observations and assessment of the stress-strain models, Constr. Build. Mater. 192 (2018) 785–797.
[118] Y.A. Al-Salloum, Influence of edge sharpness on the strength of square concrete columns confined with FRP composite laminates, Compos. B Eng. 38 (2007) 640–650.
[119] N. Chikh, M. Gahmous, R. Benzaid, Structural performance of high strength concrete columns confined with CFRP sheets, in: Proceedings of the World Congress on Engineering, 2012, pp. 4–6.
[120] A. Ilki, N. Kumbasar, Compressive behaviour of carbon fibre composite jacketed concrete with circular and non-circular cross-sections, J. Earthq. Eng. 7 (2003) 381–406.
[121] H. Toutanji, P. Balaguru, Durability characteristics of concrete columns wrapped with FRP tow sheets, J. Mater. Civil Eng. 10 (1998) 52–57.
[122] H.-J. Lin, C.-T. Chen, Strength of concrete cylinder confined by composite materials, J. Reinf. Plast. Compos. 20 (2001) 1577–1600.
[123] S. Bullo, Experimental study of the effects of the ultimate strain of fiber reinforced plastic jackets on the behavior of confined concrete, in: Proceedings of the International Conference Composites in Construction, Cosenza, Italy, 2003, pp. 16–19.
[124] T. Rousakis, R. Tepfers, Experimental investigation of concrete cylinders confined by carbon FRP sheets, under monotonic and cyclic axial compressive load, Res. Rep. 44 (2001) 1–87.
[125] M.F. Green, FRP repair of concrete structures: performance in cold regions, Int. J. Mater. Prod. Technol. 28 (2007) 160–177.
[126] S. Mandal, A. Fam, Axial loading tests on FRP confined concrete of different compressive strengths, in: Proceedings, 4th Advanced Composite Materials in Bridges and Structures, Alberta, Canada, Calgary, 2004.
[127] Q.G. Xiao, J.G. Teng, T. Yu, Behavior and modeling of confined high-strength concrete, J. Compos. Constr. 14 (2010) 249–259.
[128] T. Ozbakkaloglu, E. Akin, Behavior of FRP-confined normal-and high-strength concrete under cyclic axial compression, J. Compos. Constr. 16 (2012) 451–463.
[129] W.K. Hong, H.C. Kim, Behavior of concrete columns confined by carbon composite tube, Can. J. Civ. Eng. 31 (2) (2004) 178–188.
[130] J.C. Lim, T. Ozbakkaloglu, Hoop strains in FRP-confined concrete columns: experimental observations, Mater. Struct. 48 (2015) 2839–2854.
[131] T. Ozbakkaloglu, T. Vincent, Axial compressive behavior of circular high-strength concrete-filled FRP tubes, J. Compos. Constr. 18 (2014) 04013037.
[132] M. Saafi, H. Toutanji, Z. Li, Behavior of concrete columns confined with fiber reinforced polymer tubes, Mater. J. 96 (1999) 500–509.
[133] T. Vincent, T. Ozbakkaloglu, Influence of overlap configuration on compressive behavior of CFRP-confined normal-and high-strength concrete, Mater. Struct. 49 (2016) 1245–1268.
[134] J.C. Lim, T. Ozbakkaloglu, Influence of concrete age on stress–strain behavior of FRP-confined normal-and high-strength concrete, Constr. Build. Mater. 82 (2015) 61–70.
[135] A. Anghel, N. Papandreou, T. Parnell, A. De Palma, H. Pozidis, Benchmarking and optimization of gradient boosting decision tree algorithms, ArXiv Preprint ArXiv: 1809.04559 (2018).
[136] J.H. Friedman, Greedy function approximation: a gradient boosting machine, Ann. Stat. (2001) 1189–1232.
[137] A.V. Dorogush, V. Ershov, A. Gulin, CatBoost: gradient boosting with categorical features support, ArXiv Preprint ArXiv:1810.11363 (2018).
[138] L. Prokhorenkova, G. Gusev, A. Vorobev, A.V. Dorogush, A. Gulin, CatBoost: unbiased boosting with categorical features, Adv. Neural Inf. Process. Syst. 31 (2018).
[139] C. Bentéjac, A. Csörgő, G. Martínez-Muñoz, A comparative analysis of gradient boosting algorithms, Artif. Intell. Rev. 54 (2021) 1937–1967.
[140] S. Hussain, M.W. Mustafa, T.A. Jumani, S.K. Baloch, H. Alotaibi, I. Khan, A. Khan, A novel feature engineered-CatBoost-based supervised machine learning framework for electricity theft detection, Energy Rep. 7 (2021) 4425–4436.
[141] S.-B. Lee, Y.-J. Kim, S. Hwang, H. Son, S.K. Lee, K.-I. Park, Y.-G. Kim, Predicting Parkinson's disease using gradient boosting decision tree models with electroencephalography signals, Parkinsonism. Relat. Disord. 95 (2022) 77–85.
[142] S. Demir, E.K. Sahin, Predicting occurrence of liquefaction-induced lateral spreading using gradient boosting algorithms integrated with particle swarm optimization: pSO-XGBoost, PSO-LightGBM, and PSO-CatBoost, Acta Geotech. 18 (2023) 3403–3419.
[143] N. Pathak, B. Pohabagan, I.G.K. Mahanti, S.K. Singh, J.K. Mishra, A. Chakraborty, Synthesis of thinned planar circular array antennas using modified particle swarm optimization, System 2 (2009) 5.
[144] J. Wu, X.-Y. Chen, H. Zhang, L.-D. Xiong, H. Lei, S.-H. Deng, Hyperparameter optimization for machine learning models based on Bayesian optimization, J. Electr. Sci. Technol. 17 (2019) 26–40.
[145] W. Shafqat, S. Malik, K.-T. Lee, D.-H. Kim, PSO based optimized ensemble learning and feature selection approach for efficient energy forecast, Electronics (Basel) 10 (2021) 2188.
[146] S.M. Lundberg, S.-I. Lee, A unified approach to interpreting model predictions, Adv. Neural Inf. Process. Syst. 30 (2017).
[147] A. Altmann, L. Toloşi, O. Sander, T. Lengauer, Permutation importance: a corrected feature importance measure, Bioinformatics. 26 (2010) 1340–1347.
[148] C. Molnar, Interpretable machine learning, Lulu.com, 2020.